Nonlinear vibration control of smart plates using nonlinear modified positive position feedback approach

S. Chaman-Meymandi, A. Shooshtari*

Department of Mechanical Engineering, Engineering Faculty, Bu-Ali Sina University, Hamedan, Iran

ABSTRACT: In this paper, nonlinear vibration control of a plate is investigated using a nonlinear modified positive position feedback method that is applied through a piezoelectric layer on the plate. Based on the classical theory of displacement and strain relations with von Karman, intended equations of motion for the smart plate have been obtained. In this model, transverse vibrations are studied and stimulations are performed for the primary resonance. Boundary conditions of the smart plate are simply supported. The plate is thickness symmetrical. Using the Galerkin method the temporal nonlinear equations governing the system have been found. Then, the free and forced vibrations of the structure with the nonlinear modified positive position feedback controller have been solved using the Method of Multiple Scales to obtain an analytical solution. Results show that this controller reduces the amplitude of the vibration by inducing an increase in the damping coefficient. In addition, this provides a higher level of suppression in the overall frequency domain response by increasing the compensator gain. Finally, the results of the analytical solution for the closed-loop nonlinear modified positive position feedback controller are presented and compared with the result of the conventional positive position feedback controller and nonlinear integral resonant controller. The results show that the performance of the nonlinear modified positive position feedback controller is better than other controllers and significantly reduces the vibration amplitude.

1. INTRODUCTION

Controllers are one of the most effective ways to control linear and nonlinear vibrations. Hence, different control strategies have been presented and utilized [1]. One of the methods for nonlinear vibration control is to use active control. The advantage of using active control is its real-time adjustment according to the condition of the system and alternations in the input disturbance force on the system. To have the highest level of suppression in the vibration control process, it is essential to design a controller compatible with the nonlinear characteristics of the system oscillations. Linear and nonlinear active vibration controllers typically employ piezoelectric actuators [2]. Active vibration control is usually applied using piezoelectric ceramics as actuators and sensors, as an example, piezoelectric actuators are used in atomic force microscopes to produce high-frequency vibrations [1]. The researchers have presented the nonlinear vibration control in numerous papers. Study of Pereira and Aphal [3] ote> included a comparison between two different controllers. Omidi and Mahmoodi studied hybrid positive feedback control for active vibration attenuation of flexible structures. The structure under study in that paper is a cantilever beam, verified using numerical and experimental tests. Also, they have investigated the implementation of a modified positive velocity feedback controller for active vibration control

in smart structures [4,5]. The purpose of this study is to control the vibration suppression for a cantilever beam using a modified positive velocity feedback controller. Zhang et al. [6] also investigated nonlinear vibration suppression of the piezoelectric layer using a nonlinear modified positive position feedback approach. Tourajizadeh et al. [7] designed the optimal control for damping the unwanted vibrations of an electrostatically actuated micro-system. This configuration consists of an electro-statically actuated micro-plate attached to the end of a micro-cantilever. Vaghefpour et al. [8] attempted to derive feedback control algorithms to track a desired path of a piezoelectric size-dependent cantilever nanobeam as a nano-actuator are developed. Marinangeli et al. [9] presented the Active Vibration Control (AVC) of a rectangular carbon fibre composite plate with free edges. The plate is subjected to out-of-plane excitation by a modal vibration exciter and controlled by Macro Fibre Composite (MFC) transducers. Vibration measurements are performed by using a Laser Doppler Vibrometer (LDV) system. Sepehry et al. [10] use a novel semi-analytical method, called Scaled Boundary Finite Element Method (SBFEM), to analyze free and forced vibration of piezoelectric materials. SBFEM enables to analyze any partial derivative equation in a semi-analytical manner, however, with much lower computational cost comparing with other numerical methods. Garcia-Perez et al. [11] have reviewed asymptotic trajectory tracking

*Corresponding author's email: shooshta@basu.ac.ir

and active damping injection on a flexible-link robot by application of multiple Positive Position Feedback (PPF). Azimi et al. [12] examined active flutter control of a swept wing with an engine is carried out. The piezoelectric layers are attached to the wing to control the vibrations. Andakhshideh and Karamad. [13] studied analyzed the nonlinear dynamics of non-classical Kirchhoff microplate and chaotic behavior predicted and controlled by designing the robust adaptive fuzzy controller. Zhu et al. [14]dNote> introduced an article based on the active control of nonlinear free vibration of viscoelastic orthotropic piezoelectric doubly-curved smart nanoshells with surface effects. To achieve efficient active damping in the vibration control, a velocity feedback control law is introduced to carry out the present study.

The purpose of this paper is to obtain the equations of nonlinear vibrations and controller system for an elastic plate with a piezoelectric layer that follows the classical theory of Kirchhoff. In addition, von Karman's nonlinear strains have been used to investigate geometrical nonlinear effects. This plate has a piezoelectric layer at its upper surface. This layer actually is utilized to actively suppress the vibrations of the plate. The external force applied to the piezoelectric layer is divided into two groups: 1) the control force (Fc(t)), the control force via the controller's compensator will be logged; and 2) the harmonic excitation force distributed uniformly on the plate as the disturbance. The constitutive equations for piezoelectric layer are utilized to implement the effect of applied voltage into the electromechanical model. Method of Multiple Scales is utilized for calculation of the frequency response of the system and the controller. The resulting modulation equations are, then, used to verify the effectiveness of the proposed controller. Having the solution for the controllers, results are graphically demonstrated and discussed. In order to understand the performance of the controllers in more detail, sensitivity analysis on the closed-loop system responses is performed and the influence of each parameter on the control output has been investigated. To validate the plate equations created, the system is investigated in Ansys simulation. The results show that the frequency obtained with an acceptable error is close to the analytical value. The study of non-classical nonlinear active controllers, where actuators were designed using piezoelectric materials for nonlinear control of the system, in the past considered only for beams. As a result of the innovation in this paper, the use of non-classical nonlinear active controllers for sheets has not been analyzed to date, and most of the controllers used for sheets have been classical. Also, in the obtained plate equations, the effect of piezoelectric layer has been applied in the equations. In the previous paper, the beam equations have been used solely as a control force $f_c(t)$ as a piezoelectric effect. It should also be noted that the new controllers discussed in this paper greatly suppress jumps in the resonance zone.

2. MATHEMATICAL MODELING OF THE STRUCTURE

In this section, the nonlinear dynamic model of the structure is investigated. The structure is composed of two layers of square plates, a substructure layer, and a piezoelectric layer with different thicknesses on top of the substructure, as shown in Fig. 1. It is assumed that the h_p and h_s are thicknesses of the piezoelectric layer and substructure, respectively. Also, as shown in Fig. 1, is the side length of the plate. The origin of the coordinate system is placed on the corner of the middle plane of the substructure layer. The boundary conditions of the plate are considered as simply support and u, v and w are the displacement of the plate in the x, y and z directions, respectively.

The structure is assumed to be thin; u is the change in direction x, v change in direction y and w change in direction z. Classical Plate Theory (CPT), known as Kirchhoff theory of displacements is defined as follows [15,16]:

$$u(x,y,z) = u_0(x,y,z) - z\left(\frac{\partial w_0}{\partial x}\right) \qquad (1)$$

$$v(x,y,z) = v_0(x,y,z) - z\left(\frac{\partial w_0}{\partial y}\right) \qquad (2)$$

$$w(x,y,z) = w_0(x,y,z)$$

where u_0, v_0, w_0 are the displacements along the coordinate lines of a material point on the mid-plate.

The deflections u_0 and v_0 are associated to the extensional in-plane deformation of the plate, while w_0 denotes the transverse deflection [16]. For the assumed displacement field according to Kirchhoff's assumptions in Eq. (1), $\frac{\partial w_0}{\partial z} = 0$ hence the strain is defined as follows:

$$\begin{Bmatrix} \varepsilon_{xx} \\ \varepsilon_{yy} \\ \varepsilon_{xy} \end{Bmatrix} = \begin{Bmatrix} \varepsilon_{xx}^0 \\ \varepsilon_{yy}^0 \\ \varepsilon_{xy}^0 \end{Bmatrix} + z \begin{Bmatrix} \varepsilon_{xx}^1 \\ \varepsilon_{yy}^1 \\ \varepsilon_{xy}^1 \end{Bmatrix} \qquad (2)$$

The shear and tensile strains in the z direction are assumed zero. In Eq. (3),

$$\begin{cases} \varepsilon_{xx}^0 = \frac{\partial u_0}{\partial x} + \frac{1}{2}\left(\frac{\partial w_0}{\partial x}\right)^2 \\[2mm] \varepsilon_{yy}^0 = \frac{\partial v_0}{\partial y} + \frac{1}{2}\left(\frac{\partial w_0}{\partial y}\right)^2 \\[2mm] \varepsilon_{xy}^0 = \frac{1}{2}\left(\frac{\partial u_0}{\partial y} + \frac{\partial v_0}{\partial x} + \frac{\partial w_0}{\partial x}\frac{\partial w_0}{\partial y}\right) \end{cases}$$
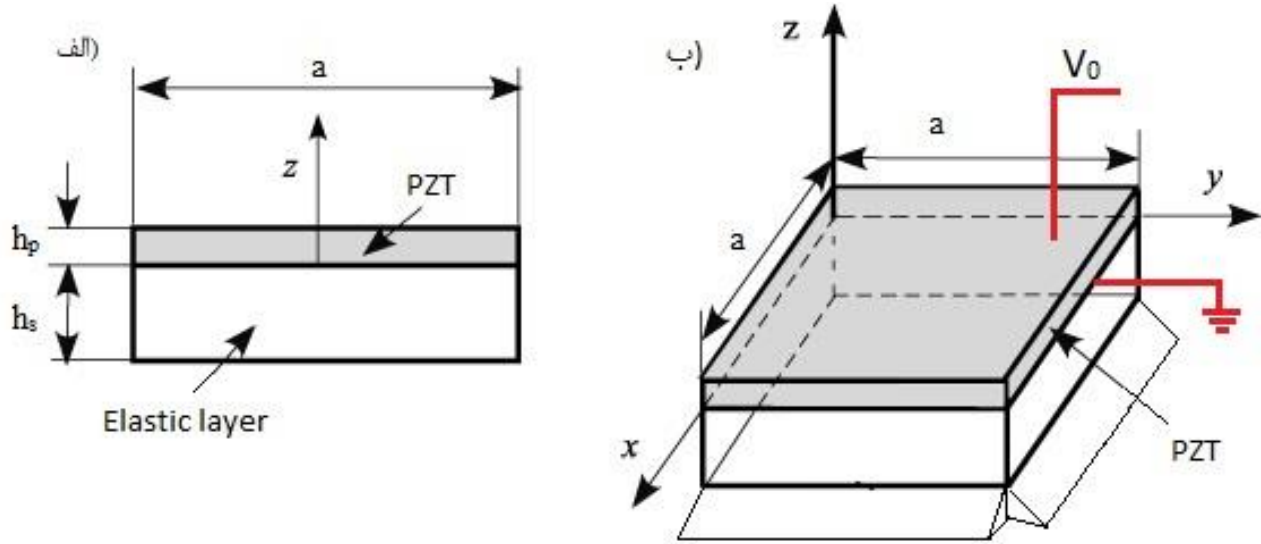
Fig. 1. The symmetric unimorph piezoelectric plate

$$\left.\begin{cases} \varepsilon_{xx}^1 = -\dfrac{\partial^2 w_0}{\partial x^2} \\[2mm] \varepsilon_{yy}^1 = -\dfrac{\partial^2 w_0}{\partial y^2} \\[2mm] \varepsilon_{xy}^1 = -\dfrac{\partial^2 w_0}{\partial x\,\partial y} \end{cases}\right. \tag{3}$$

Note that the introduced strains in Eq. (3) are known as von Karman strains in which $\{\varepsilon^0\}$ is the membrane strain and $\{\varepsilon^1\}$ is the bending strain.

The constitutive equations of isotropic piezoelectric materials can be written as [17,18]:

$$\{\sigma\} = [Q]\{\varepsilon\} - [e]\{E\}$$
$$\{D\} = [e]^T\{\varepsilon\} - [\epsilon]\{E\} \tag{4}$$

where $\{D\}, \{\sigma\}$ and $\{E\}$ are the electric field, vectors of stress and electric displacement and $[\epsilon]$ are the permittivity coefficient, respectively, $[Q]$ matrices of plane stress–reduced stiffness and $[e]$ piezoelectric coefficient. Superscript T denotes transpose of the matrix.

Also,

$$Q = \begin{bmatrix} Q_{11} & Q_{12} & 0 \\ Q_{12} & Q_{22} & 0 \\ 0 & 0 & Q_{66} \end{bmatrix} \quad e = \begin{bmatrix} 0 & 0 & e_{31} \\ 0 & 0 & e_{32} \\ 0 & 0 & 0 \end{bmatrix} \tag{5}$$

$$\varepsilon = \begin{bmatrix} \varepsilon_{11} & 0 & 0 \\ 0 & \varepsilon_{22} & 0 \\ 0 & 0 & \varepsilon_{33} \end{bmatrix} \quad \{E_e\} = \{-\psi_x, \psi_y, -\psi_z\}^T$$

In isotropic materials, the above coefficients are expressed as follows:

$$Q_{11} = Q_{22} = \frac{E_e}{1-v^2} \quad Q_{12} = vQ_{11} \quad Q_{66} = G_{12} \tag{6}$$

$$E_{e1} = E_{e2} = E_e \quad .v_1 = v_2 = v \quad .G_{12} = \frac{E_e}{2(1+v)}$$

where E_e are the elasticity modulus; v is the large Poisson's ratio; and G_{12} is the shear modulus.

Here, linear distribution of the electric potential and the thickness are assumed. For the materials examined in this study, the electric field has a significant effect on the thickness direction [15]. The z-direction electric field, E_z and that is defined as $E_z = -\dfrac{\partial \psi}{\partial z}$. ψ is the electric potential. The electric field is obtained to get the electric potential. In the process of solving these equations, it is necessary to substitute

Table 1. Properties of silicone isotropic plate

Symbol	Variable	Unit	Value
ρ_s	Density	kg/m²	2330
ϑ_s	Poisson's ratio	-	0.27
E_s	Young's modulus	GPa	160
h_s	Thickness	m	$h_s = \dfrac{2H}{3}$

Table 2. Properties of isotropic piezoelectric layer (Barium titanate (BaTiO3))

Symbol	Variable	Unit	Value
ρ_p	Density	kg/m²	5800
ϑ_p	Poisson's ratio	-	0.4639
E_p	Young's modulus	GPa	130
h_p	Thickness	m	$h_s = \dfrac{H}{3}$
$\in_{33}$	Dielectric coefficient	nC/V	12.6
$e_{31} = e_{32}$	Piezoelectric coefficient	C/m²	-4.4

Table 3. Comparing results

Mod number: mn	Ansys	Analytical Solution	Error%
1.1	8.96	9.36	4.2
1.2	37.057	37.11	0.14
1.2	55.59	56.63	0.018
1.3	80.03	83.55	4.2

the matrices expressed in Eq. (5) into Eq. (4). As a result, the axial forces and moments are defined in terms of electrical potential. The equilibrium equation is used to determine the unknown functions [19]. The electro state of the plate layers is governed by the Gauss' law for electrostatics, where k denotes the kth layer, which are:

$$D_{x,x}^{(k)} + D_{y,y}^{(k)} + D_{z,z}^{(k)} = 0 \qquad (7)$$

By substituting the value of the vector D in Eqs. (4) and (7), a linear equation is formed in terms of $\psi_{,zz}$

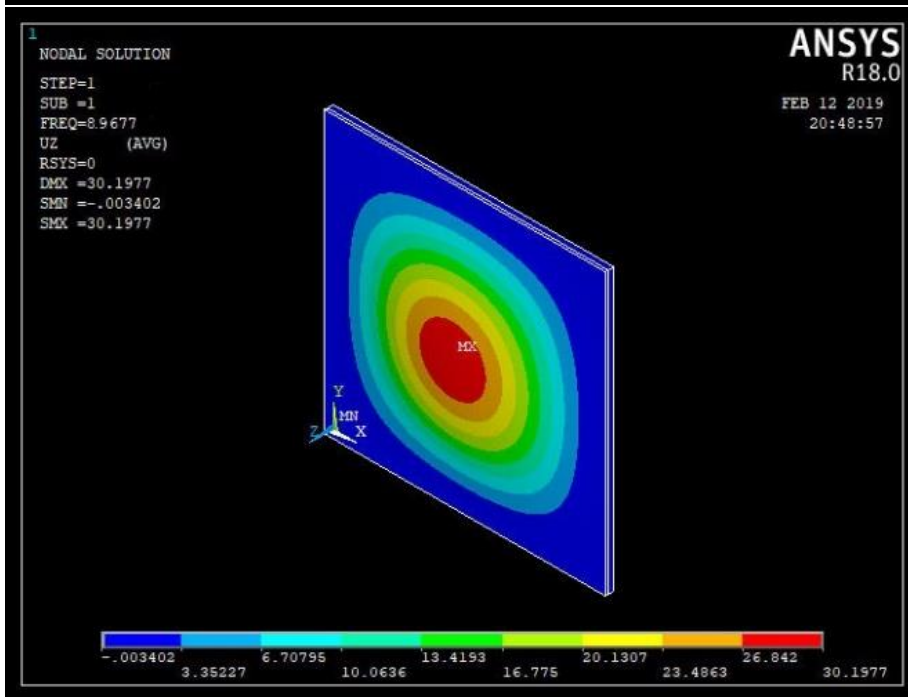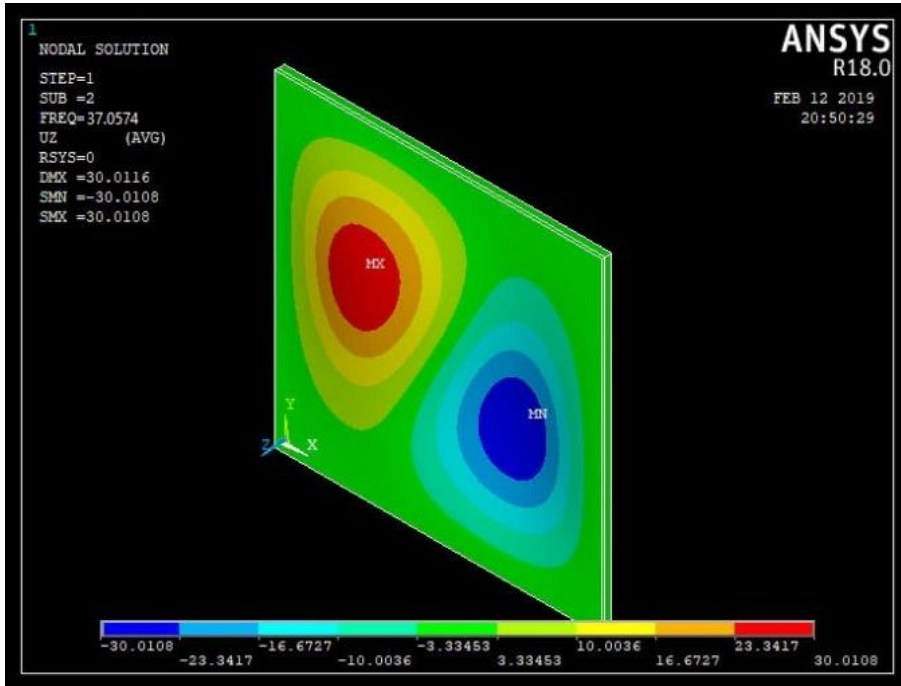$$\psi_{,zz} = \frac{1}{\partial_{33}}\left(-e_{31}w_{0,xx} - e_{32}w_{0,yy}\right) \qquad (8)$$

or

$$\psi_{,z} = \frac{1}{\partial_{33}}\left(-e_{31}w_{0,xx} - e_{32}w_{0,yy}\right)Z + \psi_0 \qquad (9)$$

where are the integration constants which are determined by enforcing the electric interface continuity conditions, i.e.

$$\psi^{(k)}\left(x,y,h_k\right) = \psi^{(k+1)}\left(x,y,h_k\right)$$

$$D_z^{(k)}\left(x,y,h_k\right) = D_z^{(k+1)}\left(x,y,h_k\right) \qquad (10)$$

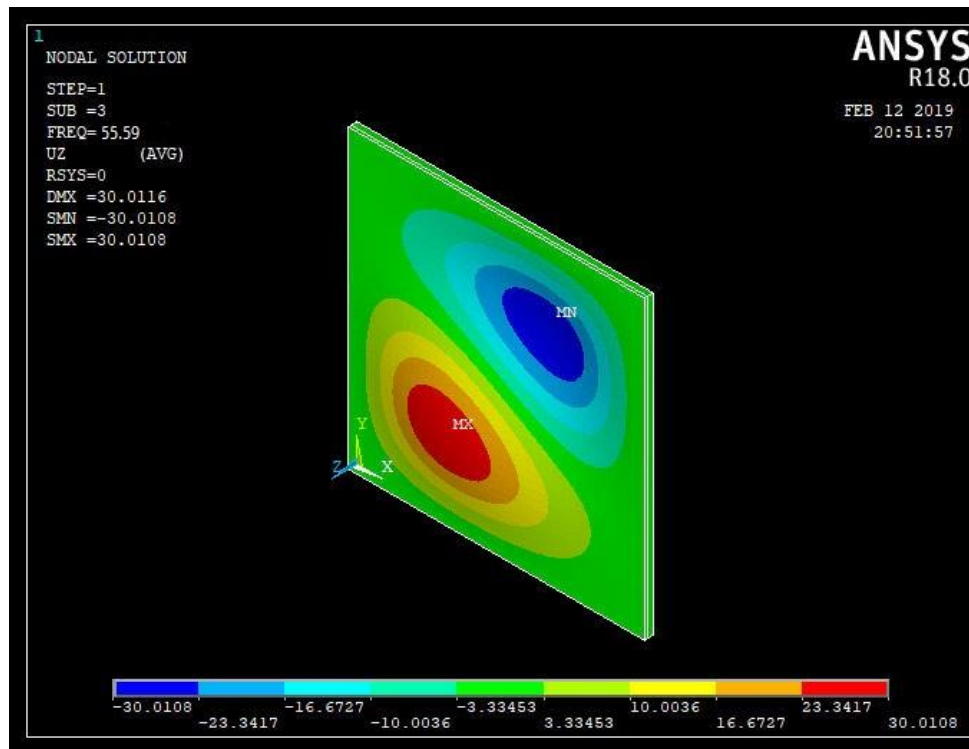and the electric boundary conditions at the top surface of the laminate which are taken to be:
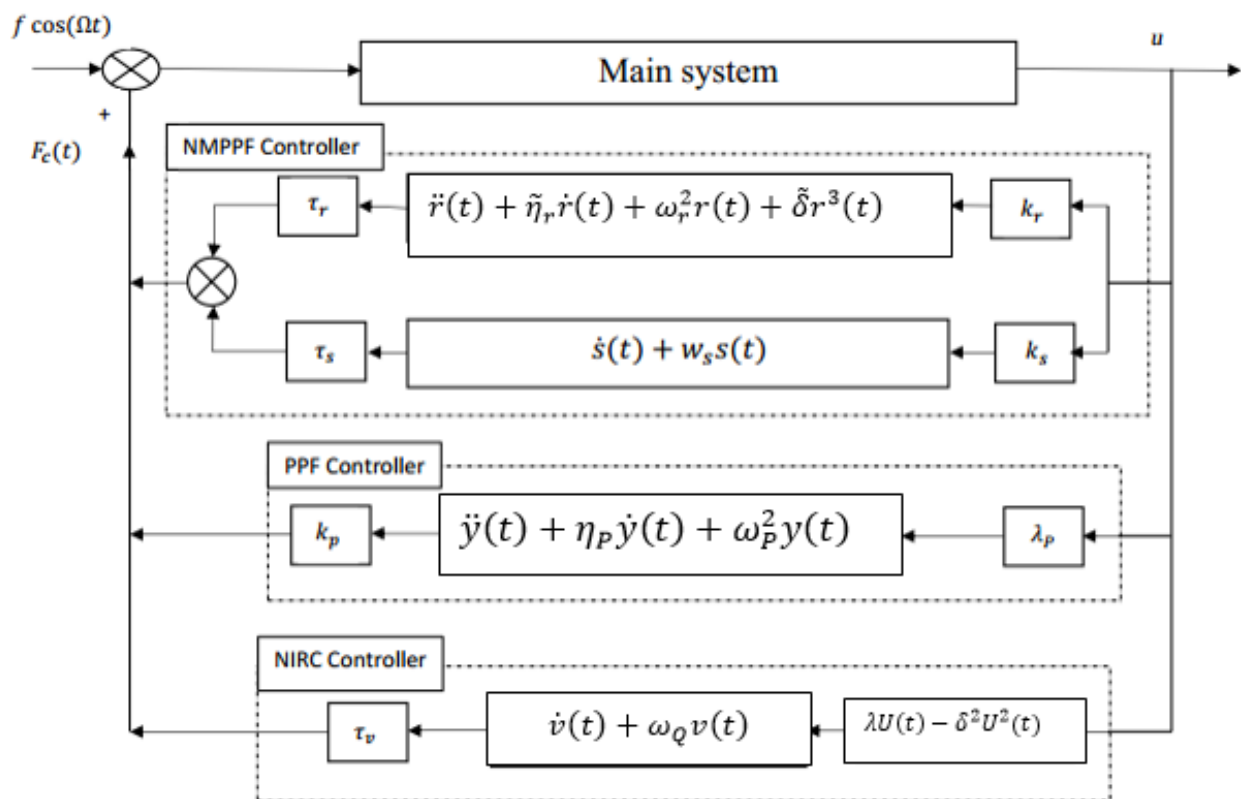
Fig. 2. displacement plate in Ansys

Fig. 3. Time-domain diagram of the NMPPF and NIRC and PPF controlled system

6

$$\psi\left(x,y,-h/2\right)=0 \qquad \psi\left(x,y,\tfrac{h}{2}\right)=v \qquad (11)$$

3. EQUATIONS OF MOTION

Using Hamilton's principle, equations of motion of the plate based on classical theory and von Karman strain–displacement relation can be obtained as [20]:

$$\frac{\partial N_{xx}}{\partial x}+\frac{\partial N_{xy}}{\partial y}=I_0\frac{\partial^2 u_0}{\partial t^2}-I_1\frac{\partial^2}{\partial t^2}\left(\frac{\partial w_0}{\partial x}\right) \qquad (12)$$

$$\frac{\partial N_{xy}}{\partial x}+\frac{\partial N_{yy}}{\partial y}=I_0\frac{\partial^2 v_0}{\partial t^2}-I_1\frac{\partial^2}{\partial t^2}\left(\frac{\partial w_0}{\partial y}\right)$$

$$\frac{\partial^2 M_{xx}}{\partial x^2}+2\frac{\partial^2 M_{xy}}{\partial x\,\partial y}+\frac{\partial^2 M_{yy}}{\partial y^2}+\frac{\partial}{\partial x}$$

$$\left(N_{xx}\frac{\partial w_0}{\partial x}+N_{xy}\frac{\partial w_0}{\partial y}\right)+\frac{\partial}{\partial y}\left(N_{xy}\frac{\partial w_0}{\partial x}+N_{yy}\frac{\partial w_0}{\partial y}\right)$$

$$+q\left(x,y,t\right)$$

$$=I_0\frac{\partial^2 w_0}{\partial t^2}+I_1\frac{\partial^2}{\partial t^2}\left(\frac{\partial u_0}{\partial x}+\frac{\partial v_0}{\partial y}\right)-I_2\frac{\partial^2}{\partial t^2}\left(\frac{\partial^2 w_0}{\partial x^2}+\frac{\partial^2 w_0}{\partial y^2}\right)$$

where q is the external excitation and $I_i=(i=1,2,3)$ are the mass moment inertias and can be expressed as

$$\begin{Bmatrix}I_0\\I_1\\I_2\end{Bmatrix}=\sum_{k=1}^{N}\int_{h_k}^{h_{k+1}}\begin{Bmatrix}1\\z\\z^2\end{Bmatrix}\rho\,dz \qquad (13)$$

where I_2,N is the rotational inertia and layer numbers. N_{xx},N_{yy},N_{xy} are in-plane forces M_{xx},M_{yy},M_{xy} are moments, which can be expressed as

$$\begin{Bmatrix}N_{xx}\\N_{yy}\\N_{xy}\end{Bmatrix}=\sum_{k=1}^{N}\int_{h_k}^{h_{k+1}}\begin{Bmatrix}\sigma_{xx}\\\sigma_{yy}\\\sigma_{xy}\end{Bmatrix}dz \qquad (14)$$

$$\begin{Bmatrix}M_{xx}\\M_{yy}\\M_{xy}\end{Bmatrix}=\sum_{k=1}^{N}\int_{h_k}^{h_{k+1}}\begin{Bmatrix}\sigma_{xx}\\\sigma_{yy}\\\sigma_{xy}\end{Bmatrix}z\,dz \qquad (15)$$

Replacing Eqs. (2), (4) in Eqs. (14) and (15), the following relations are developed,

$$\begin{Bmatrix}N_{xx}\\N_{yy}\\N_{xy}\end{Bmatrix}=\begin{bmatrix}A_{11}&A_{12}&0\\A_{12}&A_{22}&0\\0&0&A_{66}\end{bmatrix}\begin{Bmatrix}\varepsilon_{xx}^0\\\varepsilon_{yy}^0\\\varepsilon_{xy}^0\end{Bmatrix}$$

$$+\begin{bmatrix}B_{11}&B_{12}&0\\B_{12}&B_{22}&0\\0&0&B_{66}\end{bmatrix}\begin{Bmatrix}\varepsilon_{xx}^1\\\varepsilon_{yy}^1\\\varepsilon_{xy}^1\end{Bmatrix}-\begin{Bmatrix}N_{xx}^e\\N_{yy}^e\\N_{xy}^e\end{Bmatrix} \qquad (16)$$

$$\begin{Bmatrix}M_{xx}\\M_{yy}\\M_{xy}\end{Bmatrix}=\begin{bmatrix}B_{11}&B_{12}&0\\B_{12}&B_{22}&0\\0&0&B_{66}\end{bmatrix}\begin{Bmatrix}\varepsilon_{xx}^0\\\varepsilon_{yy}^0\\\varepsilon_{xy}^0\end{Bmatrix}$$

$$+\begin{bmatrix}\bar{D}_{11}&\bar{D}_{12}&0\\\bar{D}_{12}&\bar{D}_{22}&0\\0&0&\bar{D}_{66}\end{bmatrix}\begin{Bmatrix}\varepsilon_{xx}^1\\\varepsilon_{yy}^1\\\varepsilon_{xy}^1\end{Bmatrix}-\begin{Bmatrix}M_{xx}^e\\M_{yy}^e\\M_{xy}^e\end{Bmatrix} \qquad (17)$$

where

$$\left(A_{ij},B_{ij},\bar{D}_{ij}\right)=\sum_{k=1}^{N}\int_{-\frac{h}{2}}^{\frac{h}{2}}\left[Q\right]\left(1,z,z^2\right)dz \qquad (18)$$

$$\left\{N^e,M^e\right\}=\sum_{k=1}^{N}\int_{-\frac{h}{2}}^{\frac{h}{2}}\left(1,z\right)\left[e\right]\left\{E\right\}dz \qquad (19)$$

The axial motions in x and y directions have been considered negligible and only transverse vibration has been investigated; therefore, both in-pla)ne accelerations $\frac{\partial^2 v_0}{\partial t^2}$ and $\frac{\partial^2 u_0}{\partial t^2}$ can be ignored [21]. We also ignore rotational inertia. Therefore, Eq. (12) can be rewritten as:

$$\frac{\partial N_{xx}}{\partial x}+\frac{\partial N_{xy}}{\partial y}=0,\frac{\partial N_{xy}}{\partial x}+\frac{\partial N_{yy}}{\partial y}=0 \qquad (20)$$

$$\frac{\partial^2 M_{xx}}{\partial x^2}+2\frac{\partial^2 M_{xy}}{\partial x\,\partial y}+\frac{\partial^2 M_{yy}}{\partial y^2}+\frac{\partial}{\partial x}\begin{pmatrix}N_{xx}\dfrac{\partial w_0}{\partial x}+\\N_{xy}\dfrac{\partial w_0}{\partial y}\end{pmatrix}+\frac{\partial}{\partial y}$$

$$\begin{pmatrix}N_{xy}\dfrac{\partial w_0}{\partial x}\\+N_{yy}\dfrac{\partial w_0}{\partial y}\end{pmatrix}+q\left(x,y,t\right)=I_0\frac{\partial^2 w_0}{\partial t^2}-I_2\frac{\partial^2}{\partial t^2}\begin{pmatrix}\dfrac{\partial^2 w_0}{\partial x^2}+\\\dfrac{\partial^2 w_0}{\partial y^2}\end{pmatrix}$$

By introducing Airy stress function φ, in-plane relations can be defined as follows

$$\begin{cases} N_{xx} = \dfrac{\partial^2 \varphi}{\partial y^2} \\[2mm] N_{yy} = \dfrac{\partial^2 \varphi}{\partial x^2} \\[2mm] N_{xy} = -\dfrac{\partial^2 \varphi}{\partial x \partial y} \end{cases} \tag{21}$$

Presented relations in Eq. (21) satisfy the first two conditions of Eq. (20). Airy function can be determined using the following compatibility condition:

$$\frac{\partial^2 \varepsilon_{yy}^0}{\partial x^2} - \frac{\partial^2 \varepsilon_{xy}^0}{\partial x \partial y} + \frac{\partial^2 \varepsilon_{xx}^0}{\partial y^2} = \left(\frac{\partial^2 w_0}{\partial x \partial y} \right)^2$$
$$- \frac{\partial^2 w_0}{\partial x^2} \frac{\partial^2 w_0}{\partial y^2} \tag{22}$$

Also, Eq. (16) can be rewritten as:

$$\begin{Bmatrix} \varepsilon^0 \\ M \end{Bmatrix} = \begin{bmatrix} A^* & B^* \\ -\left(B^*\right)^T & D^* \end{bmatrix} \begin{Bmatrix} N \\ \varepsilon^1 \end{Bmatrix} + \begin{bmatrix} A^* & O_{3*3} \\ -\left(B^*\right)^T & -I_{3*3} \end{bmatrix}$$
$$\begin{Bmatrix} N^e \\ M^e \end{Bmatrix} \tag{23}$$

where

$$\begin{cases} A^* = A^{-1} \\ B^* = -A^{-1}B = O_{3*3} = \begin{bmatrix} 0 \end{bmatrix} \\ D^* = \bar{D} - BA^{-1}B \end{cases} \tag{24}$$

Substituting Eqs. (17), (21), (23) and (24) in Eqs. (20) and (22),

$$\bar{D}_{11} \frac{\partial^2 \varepsilon_{xx}^1}{\partial x^2} + \bar{D}_{12} \frac{\partial^2 \varepsilon_{yy}^1}{\partial x^2} + \bar{D}_{12} \frac{\partial^2 \varepsilon_{xx}^1}{\partial y^2} + \bar{D}_{22} \frac{\partial^2 \varepsilon_{yy}^1}{\partial y^2}$$
$$+ 2 \left(\bar{D}_{66} \frac{\partial^2 \varepsilon_{xy}^1}{\partial x \partial y} \right) + \left(\frac{\partial^2 \varphi}{\partial y^2} \frac{\partial^2 w_0}{\partial x^2} - \frac{\partial^2 \varphi}{\partial x \partial y} \frac{\partial^2 w_0}{\partial x \partial y} \right)$$
$$+ \left(-\frac{\partial^2 \varphi}{\partial x \partial y} \frac{\partial^2 w_0}{\partial x \partial y} + \frac{\partial^2 \varphi}{\partial x^2} \frac{\partial^2 w_0}{\partial y^2} \right) + q(x,y,t)$$
$$= I_0 \frac{\partial^2 w_0}{\partial t^2} - I_2 \frac{\partial^2}{\partial t^2} \left(\frac{\partial^2 w_0}{\partial x^2} + \frac{\partial^2 w_0}{\partial y^2} \right) \tag{25}$$

$$\frac{\partial^2}{\partial y^2} \left(A_{11}^* \frac{\partial^2 \varphi}{\partial y^2} + A_{12}^* \frac{\partial^2 \varphi}{\partial x^2} + A_{11}^* N_{xx}^e + A_{12}^* N_{yy}^e \right)$$
$$+ \frac{\partial^2}{\partial x^2} \left(A_{12}^* \frac{\partial^2 \varphi}{\partial y^2} + A_{22}^* \frac{\partial^2 \varphi}{\partial x^2} + A_{12}^* N_{xx}^e + A_{22}^* N_{yy}^e \right) \tag{26}$$
$$+ 2 A_{66}^* \frac{\partial^2}{\partial x \partial y} \left(\frac{\partial^2 \varphi}{\partial x \partial y} \right) = \left(\frac{\partial^2 w_0}{\partial x \partial y} \right)^2 - \frac{\partial^2 w_0}{\partial y^2} \frac{\partial^2 w_0}{\partial x^2}$$

By substituting obtained equation for φ from Eq. (26) in Eq. (25), a nonlinear equation for transverse plane vibrations is obtained. A boundary condition is required to solve Eq. (24). It is required to determine the boundary conditions of the problem to derive Erie's stress function and the plate transverse deformation. Here, boundary conditions are considered as a simple support. Therefore,

$$w_0 = v_0 = M_{xx} = N_{xy} = 0 \quad at \; x = 0, a$$
$$w_0 = u_0 = M_{yy} = N_{xy} = 0 \quad at \; x = 0, a \tag{27}$$

According to the boundary conditions w_0 can be defined as Equation (28):

$$w_0(x,y,t) = \sum_{n=1}^{\infty} \sum_{m=1}^{\infty} W_{mn}(t) F(x,y) =$$
$$\sum_{n=1}^{\infty} \sum_{m=1}^{\infty} W_{mn}(t) \sin\left(\frac{n\pi x}{a} \right) \sin\left(\frac{m\pi y}{b} \right) \tag{28}$$

where m and n refer to the vibrational mode number and the time variable $W_{mn}(t)$ related to the transverse deformation. According to Eq. (3), Eq. (28) can be rewritten for u_0 and v_0 as

$$u_0 = \int_0^a \varepsilon_{xx}^0 - \frac{1}{2} \left(\frac{\partial w_0}{\partial x} \right)^2 dx = 0, \quad at \; y = 0, b$$

$$\int_0^a N_{xy} dx = 0 \quad at \; y = 0, b \tag{29}$$

$$v_0 = \int_0^b \varepsilon_{yy}^0 - \frac{1}{2} \left(\frac{\partial w_0}{\partial x} \right)^2 dy = 0, \quad at \; x = 0, a$$

$$\int_0^b N_{xy} dy = 0 \quad at \; x = 0, a$$

Substituting Eq. (28) in Eq. (26) and using boundary conditions of Eq. (29), Airy function can be determined by

two particular $\left(\varphi_p\right)$ and homogeneous $\left(\varphi_h\right)$ solutions as

$$\varphi = \varphi_p + \varphi_h \tag{30}$$

The Airy stress function is expressed in Appendix A. By substituting obtained solution for Airy function in Eq. (25) and multiplying both sides in $\sin\left(\left(\dfrac{n\pi}{a}\right)x\right)\sin\left(\left(\dfrac{m\pi}{b}\right)y\right)$, then integrating over the surface of the plate (applying Galerkin method), nonlinear temporal equations can be expressed as

$$Z_1\ddot{W}(t) + Z_2 W(t) + Z_3 W^3(t) + Z_4 q = 0 \tag{31}$$

Units for coefficients of Eq. (31) have been shown in appendix B. Finally, Eq. (31) is rewritten as

$$\ddot{W}(t) + \omega_w^2 W(t) + \tilde{\alpha}W^3(t) + \tilde{\eta}_w\dot{W}(t) = \tilde{F}\cos\left(\tilde{\Omega}t\right) \tag{32}$$

The coefficients of these equations are have been defined as

$$\tilde{\alpha} = \frac{Z_2}{Z_1}, \quad \omega_w^2 = \sqrt{\frac{Z_3}{Z_1}}, \quad \tilde{F} = \frac{Z_4}{Z_1} \tag{33}$$

For Eq. (32), $W(t)$ is the time-dependent variable and $W(t)$ is a nonlinear ODE that has a third-order nonlinear term. $\tilde{F}$ and $\tilde{\Omega}$ are the excitation amplitude and frequency. $\tilde{\alpha}$ is the curvature nonlinearity coefficient. The control force $F_c(t)$, will be added to the equation. The control law that connects the controller system to the main system. $F_c(t)$ is proportional to feedback gains of compensators. $\tilde{\eta}_w$ is the damping term and the natural linear frequency of this system is ω_w^2.

ω_w^2 consists of two parts of the natural frequency created in the sheet with the piezoelectric layer and a coefficient of the voltage created from the piezoelectric layer to the elastic layer. The equation is created for the natural frequency of $\omega_w^2 = \omega^2 + s_1 V_e$ where S_1 is the constant coefficient of the voltage applied to the plate. Equations in reverse piezoelectric mode apply the initial voltage from the piezoelectric layer to the system. Also, a damping term has been added to Eq. (32) in form of $\tilde{\eta}_w = 2\tilde{\mu}_w\omega_w$ where $\tilde{\eta}_w$ is the damping ratio. It should be noted that the unit is Eq. (32) Newton's $\left[\dfrac{\text{kg.m}}{\text{s}^2}\right]$.

For dimensionless Eq. (32), need new dimensionless variables U, T that are defined as

$$T = \omega t \tag{34}$$

$$U = \frac{W}{h} \tag{35}$$

as a result

$$\ddot{U} + U + \alpha U^3 + \eta_u\dot{U} = F\cos\left(\Omega t\right) + F_c(t) \tag{36}$$

where

$$\eta_u = \frac{\tilde{\eta}_u}{\omega_u^2}, \alpha = \frac{h^2\tilde{\alpha}}{\omega_u^2}, \quad F = \frac{\tilde{F}}{h\omega_u^2}, \quad \Omega = \frac{\tilde{\Omega}}{\omega_u} \tag{37}$$

where U(t) is a nonlinear ODE equation normalized, which has third-order nonlinear terms.

4. VALIDATION OF THE DESIRED MODEL

In this section, using the finite element modeling of an elastic plate with a piezoelectric layer, the presented analytical method is confirmed. To verify the model review, the natural frequency of the structure obtained by analytical study, with the Ansys software finite element modeling are compared. The properties of the elastic plate and the piezoelectric layer are presented in Tables 1 and 2.

A double-layer plate made of Barium titanate material as a piezoelectric layer and silicone as a sub-layer has been created in Ansys. The model for this solution is the square silicone plate. Dimensions of isotropic plates are 40 × 40 cm, silicone layer thickness $h_s = 0.8$ cm and piezoelectric layer thickness $h_p = 0.4$ cm. In the model created after meshing, all four sides of the plate are limited by a simple support. The first four natural frequencies are given in Table 2 The first three eigenmodes of deformation of the plate is shown in Fig. 2.

By investigating the frequencies obtained by analytical solution, and comparing it with the simulation method, it can be seen that the results of both methods are similar, which shows the validation of the analytical method.

5. NONLINEAR CONTROLLER DESIGN AND COMPARISON

In this section, the Nonlinear Modified Positive Position Feedback (NMPPF) controller will be designed and applied to the smart plate model developed in Section 2. In addition, to evaluate and compare the controllers performance. Two other controllers i.e., Positive Position Feedback (PPF) and Nonlinear Integral Resonant Controller (NIRC) will be applied to the smart plate. The dynamical model of the nonlinear system is defined in Eq. (36). To assign a PPF control to the smart-plate, the following control model is utilized [22]

$$\ddot{y}(t) + \eta_P \dot{y}(t) + \omega_P^2 y(t) = \lambda_P U(t) \tag{38}$$

where $y(t)$ is a positive position feedback controller variable. In this equation, the attenuation coefficient is, $\eta_p = 2\mu_p\omega_p$, in which μ_p is the damping ratio, and ω_p is the positive feedback controller frequency. $\lambda_p > 0$ is the controller gain, and feedback loop is closed by setting $F_c(t) = k_p y(t)$ in Eq. (36), for $k_p > 0$. Where k_p positive scalar feedback gains of first-order compensator. The NIRC controller model is expressed as [23]

$$\dot{v}(t) + \omega_Q v(t) = \lambda U(t) - \delta^2 U^2(t) \tag{39}$$

where $v(t)$ is NIRC controller's variable, ω_Q is the first-order integrator's frequency. λ and δ are the controller input gains. The control law is defined as $F_c = \tau_v v(t)$ for $\tau_v > 0$.

The NMPPF are designed as follows. This controller includes a nonlinear second-order compensator and a linear first-order compensator set in parallel. As the system is a third-order nonlinear system, the third-order nonlinear expression controller is considered in the second-order compensator [1]

$$\ddot{\overline{r}}(t) + \tilde{\eta}_r \dot{\overline{r}}(t) + \omega_r^2 \overline{r}(t) + \tilde{\delta}\overline{r^3}(t) = \tilde{k}_r U(t) \tag{40}$$

$$\dot{\overline{s}}(t) + \omega_s \overline{s}(t) = \tilde{k}_s U(t)$$

where $\overline{r}(t)$ and $\overline{s}(t)$ are compensatory first and second order state variables, respectively. $\tilde{\eta}_r = 2\mu_r\omega_r$, when μ_r is the coefficient of damping, and ω_r is the compensating frequency. k_r and k_s are the inputs of the control. The control law pertains to the modified positive position feedback controls system in the main system of Eq. (36) as $F_c(t) = \tau_r r(t) + \tau_s s(t)$; that are τ_r and τ_s respectively, are first order compensator and second in a closed loop system.

Fig. 3 shows linear and nonlinear feedback controllers, including all three control methods for the closed loop system. It should be mentioned that controllers are used one at a time and not together as shown in Fig. 3.

6. NMPPF CONTROLLER FOR SMART PLATE
The method of Multiple Time Scales is used to find a uniform nonlinear structure: the approximate solution to the resonance structure [24]. The nonlinear system of Eq. (36) under NMPPF controllers are defined as follows: analyzing the nonlinear system of Eq. (36), which is governed by the NMPPF controller of expressed in Eq. (40), we need new dimensionless variable for controllers so Eq. (40) becomes dimensionless like Eq. (36). The result is as follows

$$\ddot{r} + r + \delta r^3 + \eta_r \dot{r} = k_r U \tag{41}$$

$$\dot{s} + s = k_s U$$

where

$$\eta_r = \frac{\tilde{\eta}_r}{\omega_r} \ , \ \delta = \frac{h^2\tilde{\delta}}{\omega_r^2} \ , k_r = \frac{\tilde{k}_r}{\omega_r^2} \ , k_s = \frac{\tilde{k}_s}{\omega_s} \tag{42}$$

In the primary resonance case, excitation frequency (Ω) is assumed as follows $\Omega = 1 + \varepsilon\sigma_f$.

To this end, two time-scales of $T_0 = t$, $T_1 = \varepsilon t$ are selected. Then, the time derivatives are defined as

$$\frac{d}{dt} = D_0 + \varepsilon D_1 + \dots \ , \quad \frac{d^2}{dt^2} = D_0^2 \tag{43}$$
$$+ 2\varepsilon D_0 D_1 + \dots$$

where $D_n = \frac{\partial}{\partial T_n}$, and $\varepsilon = \left(\frac{h}{\omega}\right)^2$ is a bookkeeping parameter. Eq. (43) is substituted in Eqs. (36), (41) that results in

$$D_0^2 U_0 + 2\varepsilon D_0 D_1 U_1 + \eta_U D_0 U_0 + \varepsilon\eta_U D_1 U_1 + U_0 + \varepsilon U_1$$
$$+ \alpha(U_0 + \varepsilon U_1)^3 + \dots = f\cos(\Omega t) + \tau_r r + \tau_s s, \tag{44}$$

$$D_0^2 r + 2\varepsilon D_0 D_1 r + \eta_r D_0 r + \varepsilon\eta_r D_1 r + r + \delta r^3$$
$$+ \dots = k_r U, \tag{45}$$

$$D_0 s + \varepsilon D_1 s + s + \dots = k_s U \tag{46}$$

Parameters of the equations have to be scaled; therefore, parameters are set as:

$$\alpha = \varepsilon\hat{\alpha} \ , k_r = \varepsilon\widehat{k_r} \ , k_s = \widehat{k_s} \ , \tau_r = \varepsilon\widehat{\tau_r} \ , \tau_s = \varepsilon\widehat{\tau_s}$$
$$\eta_r = \varepsilon\widehat{\eta_r} \ , \delta = \varepsilon\hat{\delta} \ , f = \varepsilon\hat{f}$$

Scaled parameters are substituted into the Eqs. (44) to (46), then the variables $U(t), r(t)$ and $s(t)$ are expanded by

$$U(\varepsilon T_0, T_1) = U_0(T_0, T_1) + \varepsilon U_1(T_0, T_1) + \dots, \tag{47}$$

$$r\left(\varepsilon T_0 T_1\right) = r_0\left(T_0 T_1\right) + \varepsilon r_1\left(T_0 T_1\right) + \ldots , \qquad (48)$$

$$s\left(\varepsilon T_0 T_1\right) = \varepsilon s_0\left(T_0 T_1\right) + \varepsilon^2 s_1\left(T_0 T_1\right) + \ldots . \qquad (49)$$

By placing Eqs. (44), (45) and (46) in Eqs. (47), (48) and (49) and ordering the result in terms of the power of ε^0, ε^1 and ε^2, the following differential equations are obtained.

$$O\left(\varepsilon^0\right): \quad D_0^2 U_0 + U_0 = 0 , \qquad (50)$$

$$D_0^2 r_0 + r_0 = 0 \qquad (51)$$

$$O\left(\varepsilon^1\right): \quad D_0^2 U_1 + U_1 = \hat{f}\cos\left(\Omega t\right) + \hat{\tau}_r r_0 + \hat{\tau}_s s_0 \qquad (52)$$
$$-2D_0 D_1 U_0 - \hat{\eta}_u D_0 U_0 - \hat{\alpha} U_0^3 ,$$

$$D_0^2 r_1 + r_1 = \hat{k}_r U_0 - 2D_0 D_1 r_0 \qquad (53)$$
$$-\hat{\eta}_r D_0 r_0 - \hat{\delta} r_0^3 .$$

$$D_0 s_0 + s_0 = \hat{k}_s U_0 \qquad (54)$$

$$O\left(\varepsilon^2\right): \quad D_0 s_1 + s_1 = \hat{k}_s U_1 + D_1 s_0 , \qquad (55)$$

The order ε^2 is considered for s only as function based on Eq. (49) includes the orders of ε^1 and ε^2.

$$U_0 = A\left(T_1\right)e^{iT_0} + cc , \qquad (56)$$

$$r_0 = B\left(T_1\right)e^{iT_0} + cc , \qquad (57)$$

Thus, $A\left(T_1\right), B\left(T_1\right)$ are complex parameters functions that will be defined by deface the secular terms, also where U_0 domain is r_0, which is a function of function T_1.

$$s_0 = C\left(T_1\right)e^{iT_0} + \frac{\hat{k}_s}{2}\left(1 - i\right)A\left(T_1\right)e^{iT_0} + cc \qquad (58)$$

Thus, $C\left(T_1\right)$ is obtained in the next steps. At this step, Eqs. (56) to (58) are inserted into Eqs. (52), (53): Ultimately, the results are simplified as follows.

$$D_0^2 U_1 + U_1 = \hat{\tau}_r B\left(T_1\right)e^{iT_0} - \left(\hat{\eta}_u A\left(T_1\right) + 2D_1 A\left(T_1\right)\right)$$
$$ie^{iT_0} + \hat{\tau}_s\left(C\left(T_1\right)e^{-T_0} + \frac{\hat{k}_s}{2}\left(1 - i\right)A\left(T_1\right)e^{iT_0}\right) \qquad (59)$$
$$-\hat{\alpha}A^3\left(T_1\right)e^{i 3T_0} - 3\hat{\alpha}A^2\bar{A}e^{iT_0} + \frac{\hat{f}}{2}e^{i\Omega T_0} + cc$$

$$D_0^2 r_1 + r_1 = \hat{k}_r A\left(T_1\right)e^{iT_0} - \hat{\delta}B^3\left(T_1\right)e^{i 3T_0} \qquad (60)$$
$$-3\hat{\delta}B^2\bar{B}\left(T_1\right)e^{iT_0} - \left(\hat{\eta}_r B\left(T_1\right) + 2D_1 B\left(T_1\right)\right)ie^{iT_0}$$

U_1 and r_1 are calculated using Eqs. (59) and (60) in time domain. Eq. (58) and U_1 have been substituted in Eq. (55) for creating ODE equations to solve the equation. Moreover, the term cc shows the complex conjugate function of its preceding sentences.

For the system to have a bounded solution, it must be considered zero to the secular terms. Applying this condition to the expanded Eq. (55) and using U_1, $C\left(T_1\right)$ is calculated as

$$C\left(T_1\right) = c_s e^{\left(\frac{\hat{k}_s \hat{\tau}_s}{2}\right)T_1} \qquad (61)$$

where c_s is a constant. Next step is to sort Eqs. (59) and (60), and separate the secular terms,

$$\begin{bmatrix} \hat{\tau}_r B\left(T_1\right)e^{i\sigma_r T_1} + \\ \dfrac{\hat{\tau}_s \hat{k}_s}{2}\left(\omega_s - i\right)A\left(T_1\right) \\ -\left(\hat{\eta}_u A\left(T_1\right) + 2D_1 A\left(T_1\right)\right)i \\ +\dfrac{\hat{f}}{2}e^{i\sigma_f T_1} - A^2\left(T_1\right)\bar{A}\left(T_1\right)3\hat{\alpha} \end{bmatrix} e^{iT_0} = 0 , \qquad (62)$$

$$\begin{bmatrix} \hat{k}_r A\left(T_1\right)e^{-i\sigma_r T_r} - 3\hat{\delta}B^2\left(T_1\right)\bar{B}\left(T_1\right) \\ -\left(\hat{\eta}_r B\left(T_1\right) + 2D_1 B\left(T_1\right)\right)i \end{bmatrix} e^{i\omega_r T_0} = 0, \qquad (63)$$

The solution to Eqs. (62) and (63) is assumed in the polar form of

$$A\left(T_1\right) = \frac{1}{2}a\left(T_1\right)e^{i\zeta_a\left(T_1\right)}, \qquad (64)$$

Table 4. Numerical values of the main system parameters

Variable	α	μ_u	ω_u
Value	11.7	0.03	9.36

Table 5. Numerical values of the PPF controller parameters

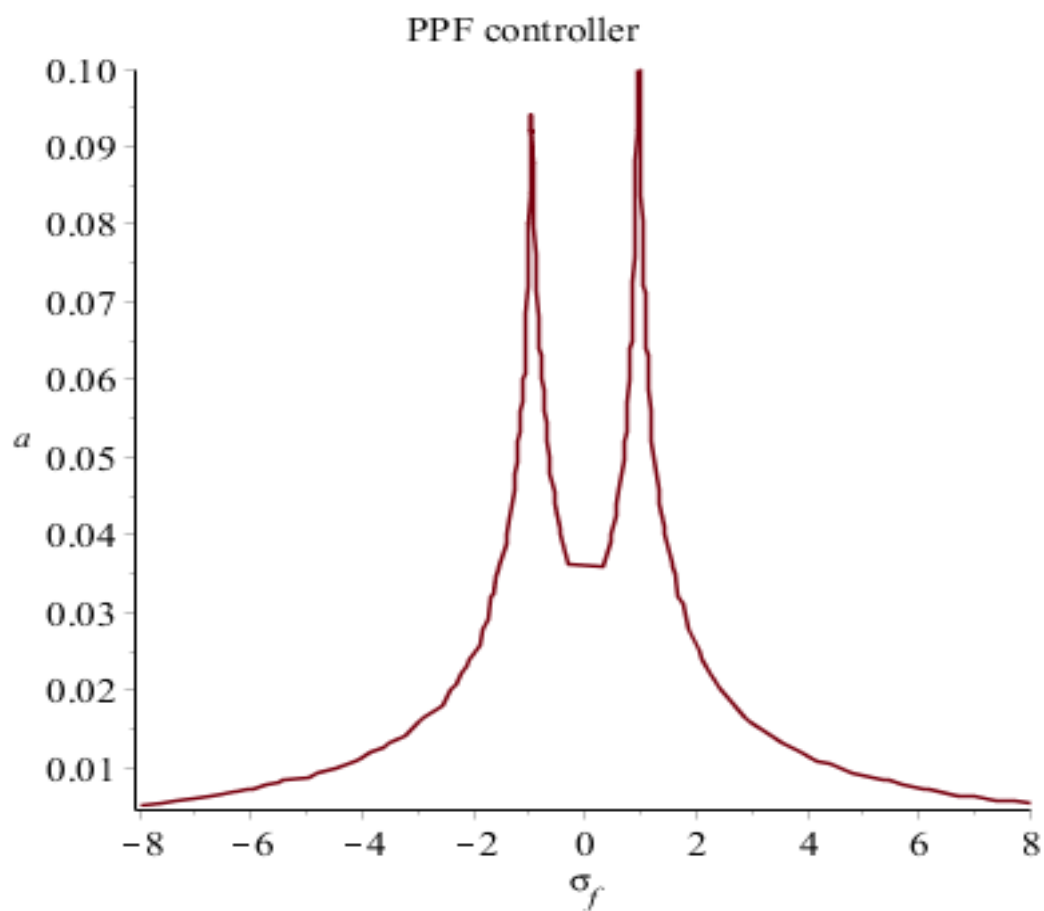| Variable	λ_p	k_p	μ_p	ω_p	F
Value	1	1	0.002	9.36	0.09
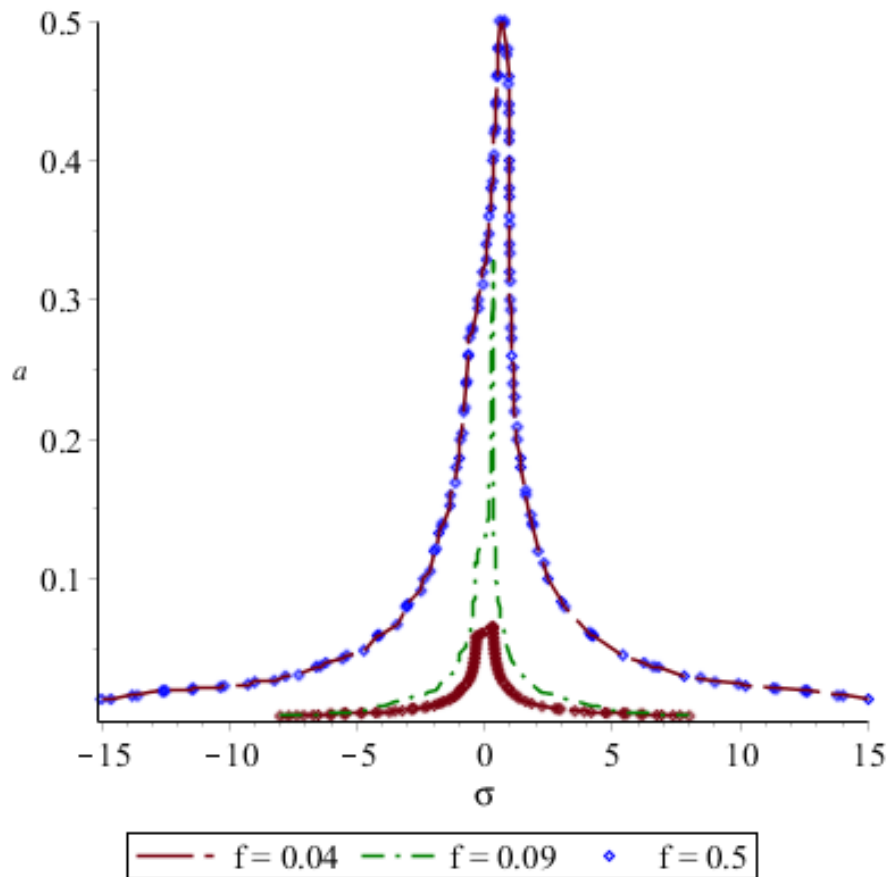
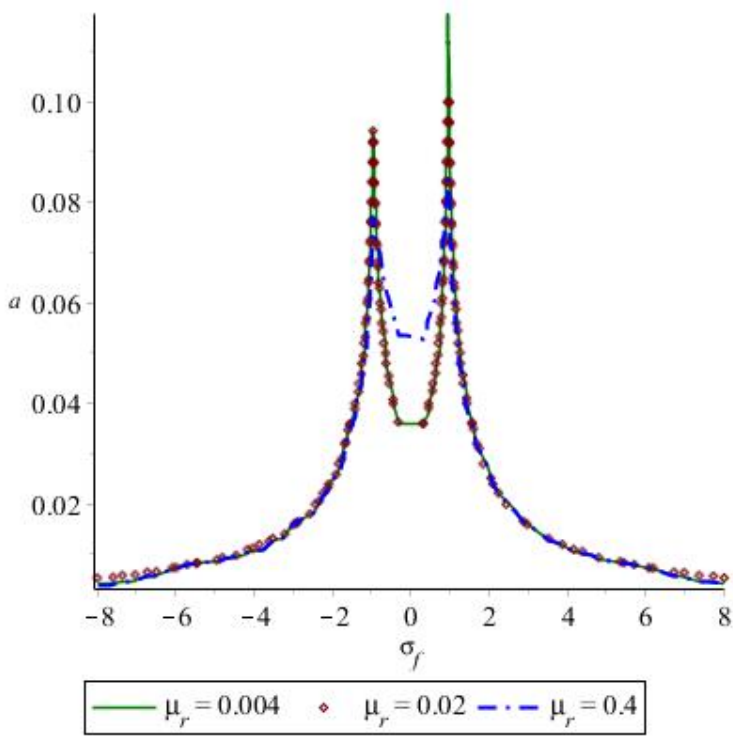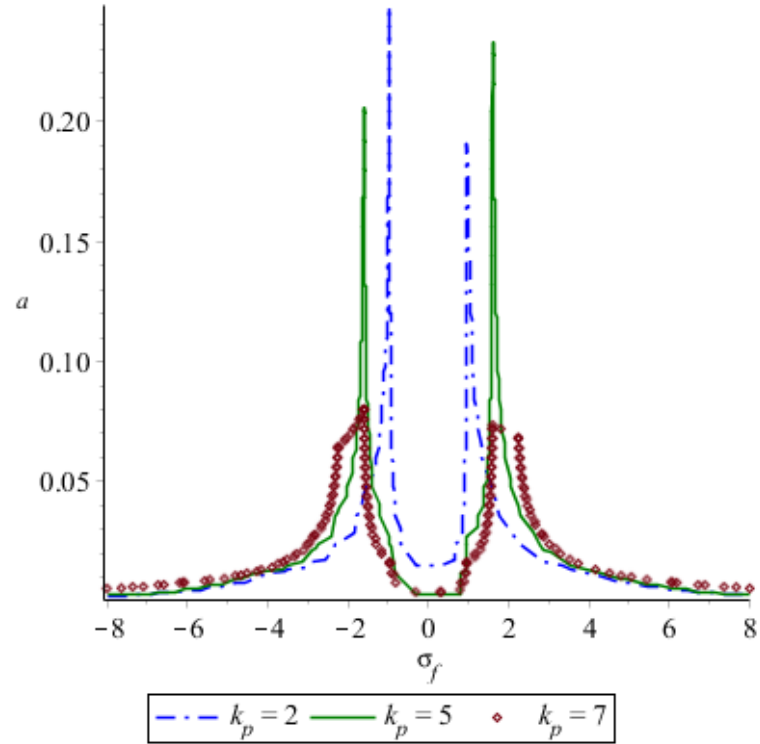**Fig. 4. Frequency response of the uncontrolled system**
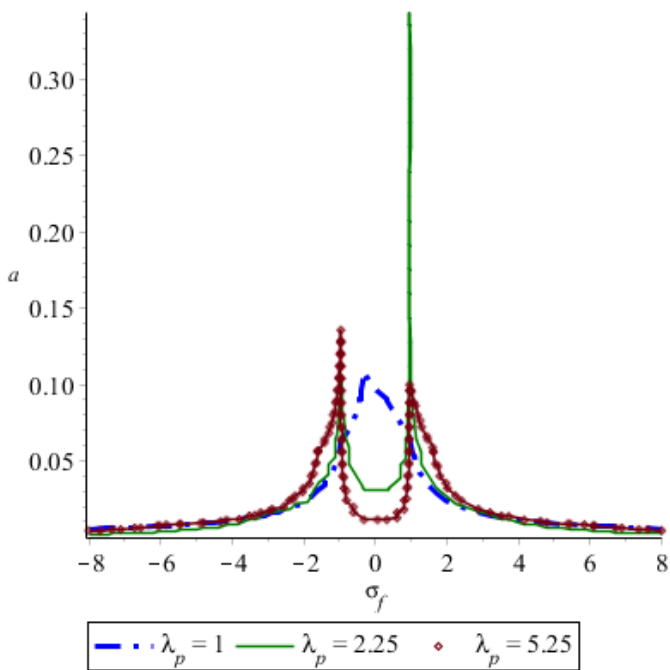
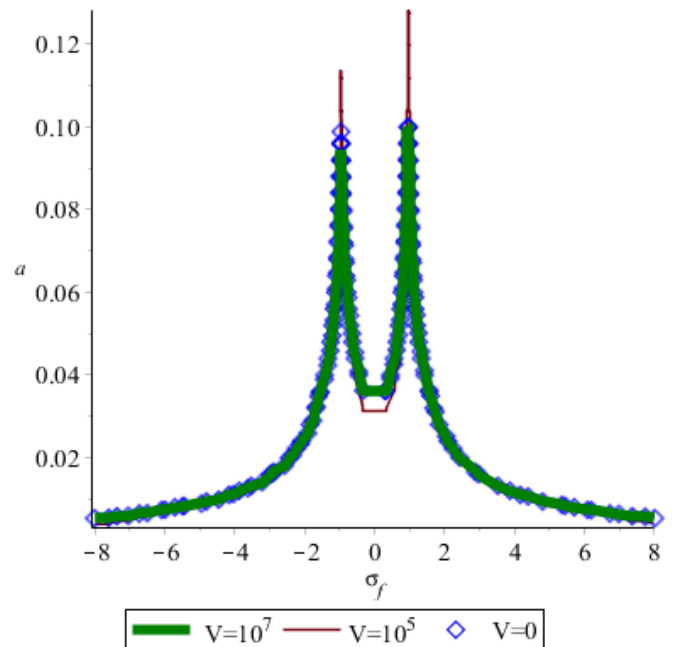**Fig. 5. Frequency response of the PPF controlled**

(a)

(b)

(c)

(d)

Fig. 6. Sensitivity analysis of the closed-loop PPF controlled system to control parameters. (a) damping coefficient $\left(\mu_r\right)$, (b) control gain $\left(\lambda_p\right)$, (c) control gain $\left(k_p\right)$, (d) voltage $\left(V\right)$

$$B\left(T_1\right) = \frac{1}{2}b\left(T_1\right)e^{i\zeta_b(T_1)}, \tag{65}$$

The real and imaginary parts will be separated and equal to zero by placing Eqs. (64) and (65) in Eqs. (62) and (63) The following equations are obtained.

$$D_1 a\left(T_1\right) = -\frac{\hat{\tau}_s \hat{k}_s}{2}a\left(T_1\right) + \frac{\hat{f}}{2}\sin\left(\begin{array}{c}\sigma_f T_1 \\ -\zeta_a\left(T_1\right)\end{array}\right)$$

$$+\frac{\hat{\tau}_r}{2}b\left(T_1\right)\sin\left(\sigma_r T_1 + \zeta_b\left(T_1\right) - \zeta_a\left(T_1\right)\right) \tag{66}$$

$$-\frac{\hat{\eta}_u}{2}a\left(T_1\right)$$

$$D_1\zeta_a\left(T_1\right) = \frac{3\hat{\alpha}}{8}a^2\left(T_1\right) - \frac{\hat{f}}{2a\left(T_1\right)}\cos\left(\begin{array}{c}\sigma_f\left(T_1\right) \\ -\zeta_a\left(T_1\right)\end{array}\right)$$

$$-\frac{\hat{\tau}_r b\left(T_1\right)}{2a\left(T_1\right)}\cos\left(\left(\begin{array}{c}\sigma_r\left(T_1\right) + \zeta_b\left(T_1\right) \\ -\zeta_a\left(T_1\right)\end{array}\right)\right) - \frac{\hat{\tau}_s \hat{k}_s}{2} \tag{67}$$

$$D_1 b\left(T_1\right) = -\frac{\hat{\eta}_r}{2}b\left(T_1\right) + \frac{\hat{k}_r}{2}a$$

$$\left(T_1\right)\sin\left(\left(\zeta_a\left(T_1\right) - \sigma_r T_1 - \zeta_b\left(T_1\right)\right)\right) \tag{68}$$

$$D_1\zeta_b\left(T_1\right) = -\frac{3\hat{\delta}}{8}b^2\left(T_1\right) + \frac{\hat{k}_r a\left(T_1\right)}{2b\left(T_1\right)}$$

$$\cos\left(\left(\zeta_a\left(T_1\right) - \sigma_r T_1 - \zeta_b\left(T_1\right)\right)\right) \tag{69}$$

Since all variables of Eqs. (66) to (66) are time derivatives of T_1 function. New variables are defined, as follows to obtain the set of independent equation

$$\theta_a\left(t\right) = \sigma_f t - \zeta_a\left(t\right) \text{ and } \theta_b\left(t\right) = \sigma_r t + \zeta_b\left(t\right) - \zeta_a\left(t\right)$$

. by applying these changes, the modulation equation is obtained as follows.

$$\dot{a} = -\left(\frac{\hat{\eta}_u}{2} + \frac{\hat{\tau}_s \hat{k}_s}{2}\right)a +$$

$$\frac{\hat{f}}{2}\sin\left(\theta_a\right) + \frac{\hat{\tau}_r}{2}b\sin\left(\theta_a\right) \tag{70}$$

$$\dot{\theta}_a = -\frac{3\hat{\alpha}}{8}a^2 + \frac{\hat{\tau}_s \hat{k}_s}{2} +$$

$$\frac{\hat{f}}{2}\frac{1}{a}\cos\left(\theta_a\right) + \frac{\hat{\tau}_r}{2}\frac{b}{a}\cos\left(\theta_b\right) + \sigma_f \tag{71}$$

$$\dot{b} = -\frac{\hat{\eta}_r}{2}b - \frac{\hat{k}_r}{2}a\sin\left(\theta_b\right) \tag{72}$$

$$\dot{\theta}_b = \frac{3\hat{\delta}}{8}b^2 + \frac{\hat{f}}{2}\frac{1}{a}\cos\left(\theta_a\right) +$$

$$\left(\frac{\hat{\tau}_r b}{2a} - \frac{\hat{k}_r a}{2b}\right)\cos\left(\theta_b\right) - \frac{3\hat{\alpha}}{8}a^2 + \frac{\hat{\tau}_s \hat{k}_s}{2} + \sigma_r \tag{73}$$

steady-state conditions are considered to obtain the frequency response of the closed loop system. The coupled equations obtained for the frequency are the response of the main system and the controller domain.

$$\left(\frac{\hat{f}}{2}\right)^2 = \left[\left(\frac{\hat{\eta}_u}{2} + \frac{\hat{\tau}_s \hat{k}_s}{2}\right)a + \frac{\hat{\tau}_r \hat{\eta}_r b^2}{2k_r a}\right]^2$$

$$+ \left[\begin{array}{c}\frac{3\hat{\alpha}}{8}a^3 + \frac{\hat{\tau}_s \hat{k}_s}{2}a - \frac{3\hat{\delta}\hat{\tau}_r}{8\hat{k}_r}\frac{b^4}{a} - \frac{\hat{\tau}_r}{\hat{k}_r} \\ \left(\sigma_r - \sigma_f\right)\frac{b^2}{a} - \sigma_f a\end{array}\right]^2 \tag{74}$$

$$\left[1 - \frac{\hat{\eta}_r^2}{\hat{k}_r^2}\frac{b^2}{a^2}\right]^{\frac{1}{2}} = \frac{3\hat{\delta}}{4\hat{k}_r}\frac{b^3}{a} + \frac{2}{\hat{k}_r}\left(\sigma_r - \sigma_f\right)\frac{b}{a}. \tag{75}$$

7. RESULTS AND DISCUSSIONS

This part has discussed the vibration range in the resonant frequency region and the performance of the controllers in controlling the vibration amplitude in the resonance region are discussed and its details.

7.1. Open-Loop System Response Under Primary Resonance

It is necessary to provide an image of the system reaction in an uncontrolled mode prior to studying the closed loop system. The open-loop system is obtained from Eqs. (74) and (75). The values of the main system are given in Table 4 and the frequency response graph in Fig. 4. System behavior is defined for the excitation force $f = 0.09$ [N]. The jump phenomenon is seen in the excitation range. The purpose of the controllers is to diminish the maximum vibration range in the frequency domain. Using analytical relations and structural dimensions simulated in Ansys, the values of the desired parameters are obtained.

7.2. Ppf Controller Performance Analysis

This part examined the performance of the closed loop system with PPF controller [1,22]. The equations of the PPF controller frequency response equations are shown as the NMPPF controller by the multiple time scale approach. These equations are obtained by forms Eqs. (76) and (77). Fig. 5
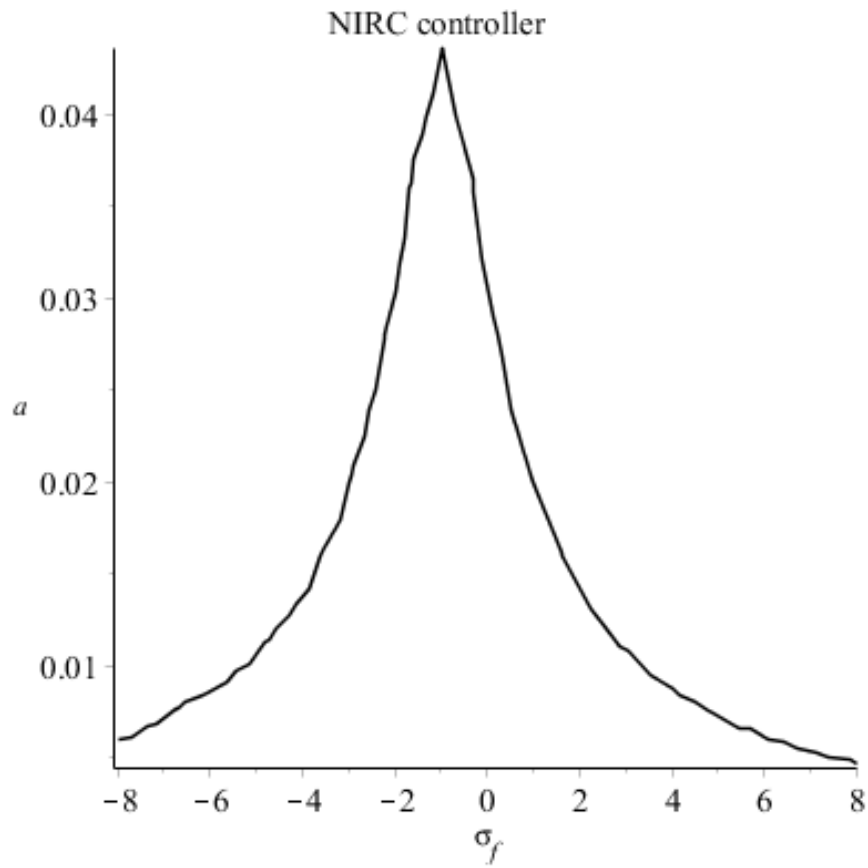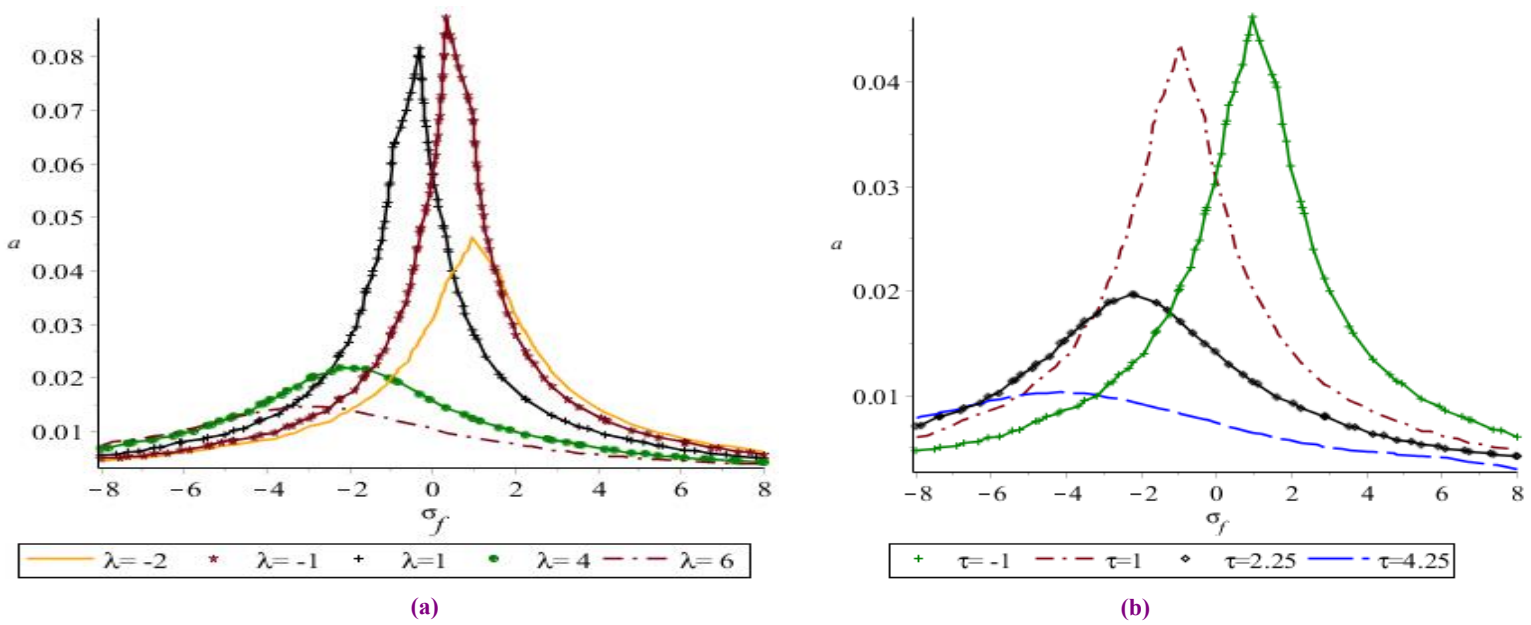
Fig. 7. Frequency response of the NIRC controlled

Fig. 8. NIRC controlled system response for changes in excitation amplitude. (a) controller input gain (λ), (b) controller input gains (τ).
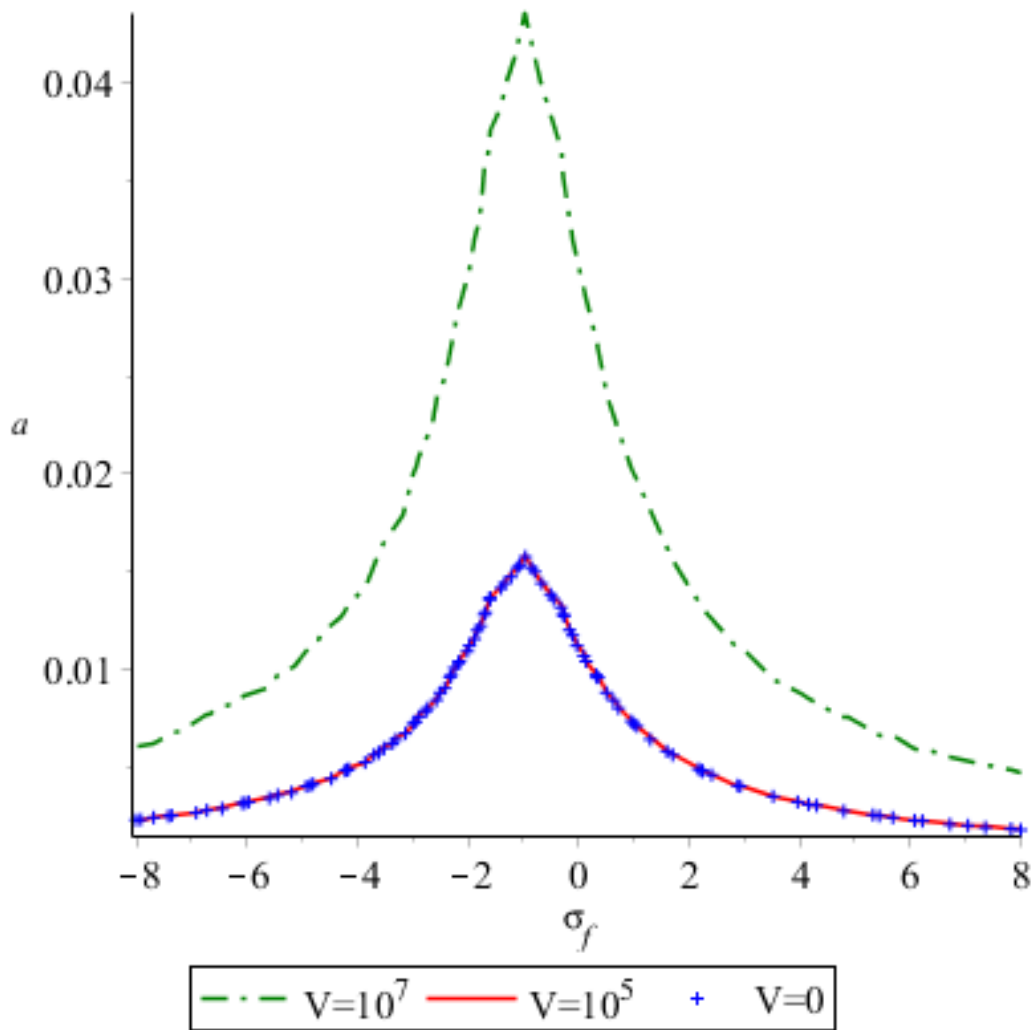
Fig. 9. The effect of the voltage on the NIRC

Table 6. Numerical values of the NIRC controller parameters

Variable	ω_Q	λ	δ	τ_v	f
Value	9.36	2	0	1	0.09

Table 7. Numerical values of the NMPPF controller

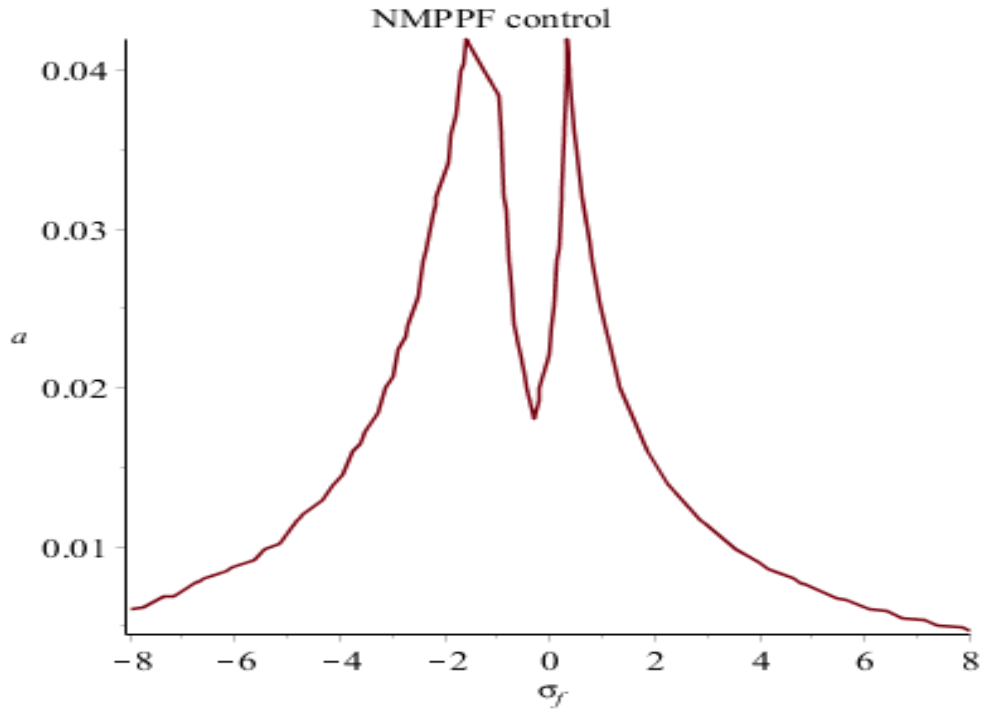| Variable	ω_r	ω_s	μ_r	δ	k_r	τ_r	k_s	τ_s	f
Value	9.36	9.36	0.002	0	2	1	2	1	0.09

17

Fig. 10. Frequency response of the NMPPF controlled system
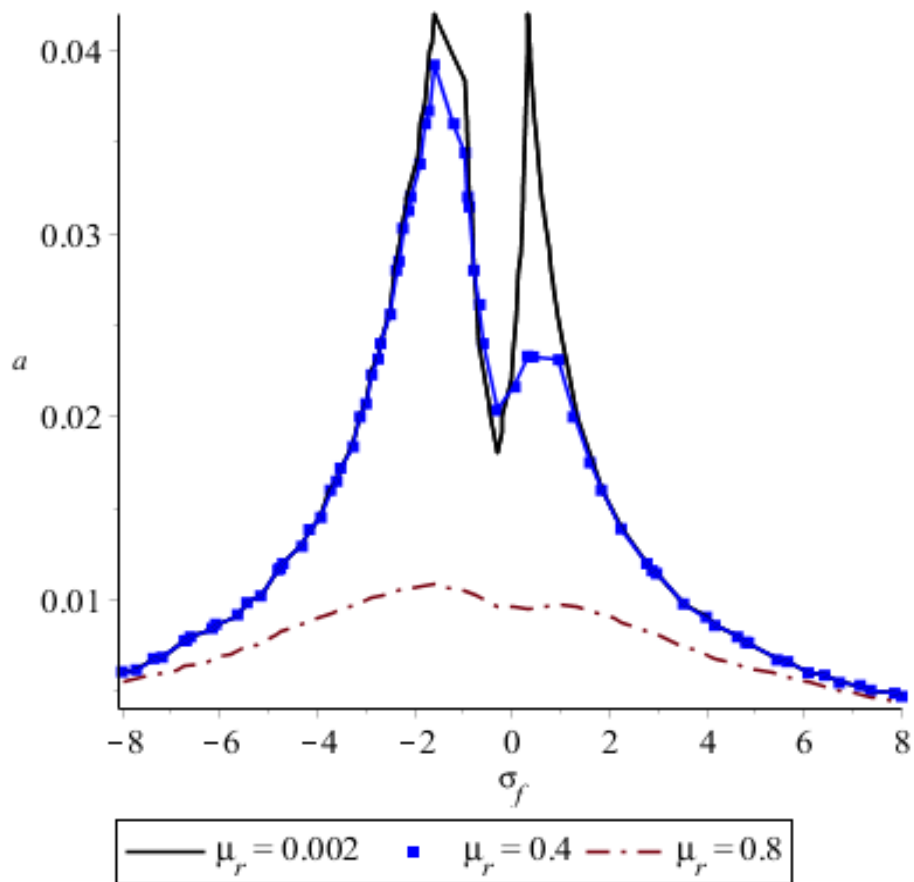
Fig. 11. Frequency response of the closed-loop system for values of damping ratio
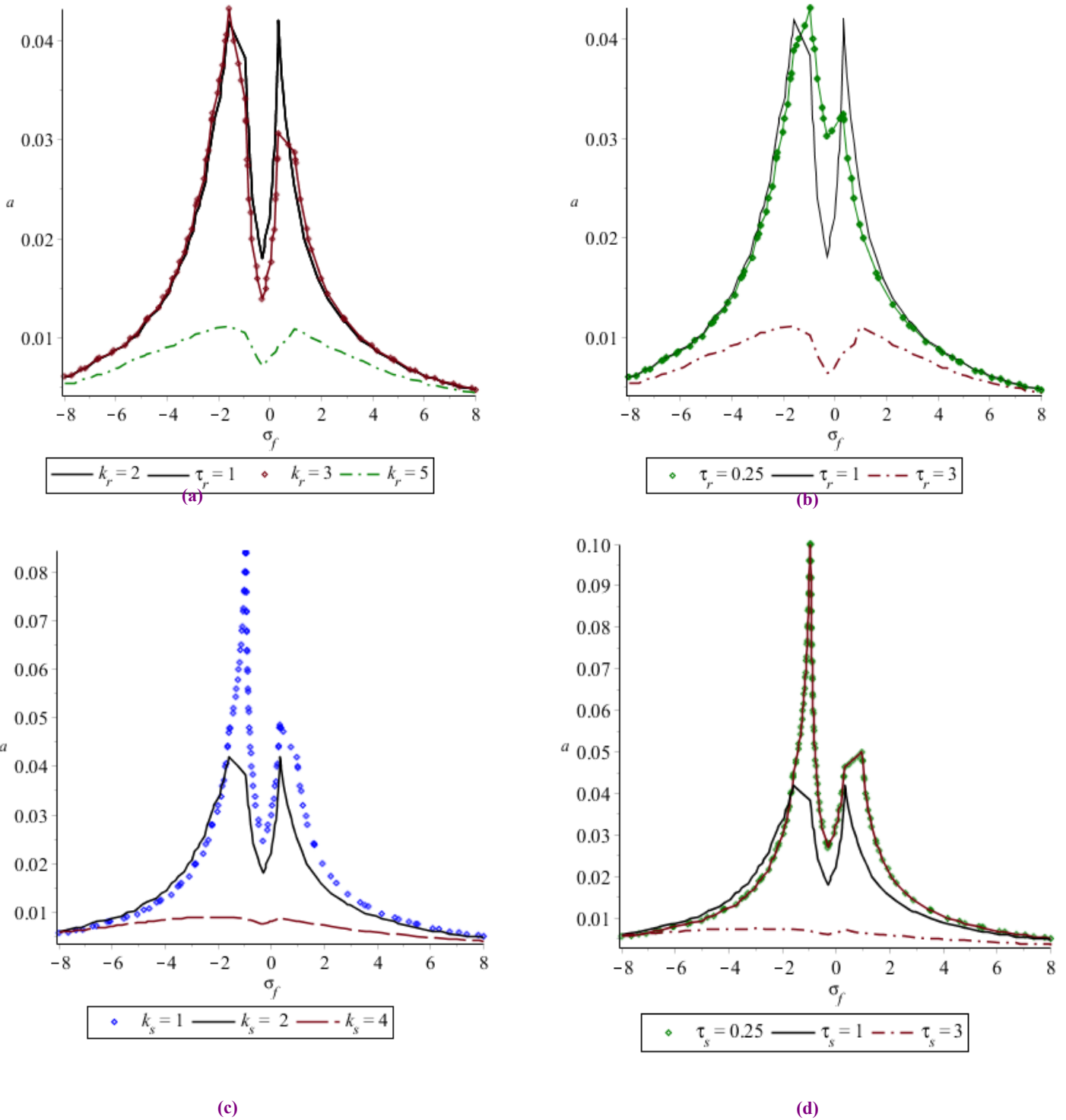
Fig. 12. Sensitivity of the closed-loop NMPPF controlled system response. (a) controller input gain for the second order (k_r), (b) gain for the second order compensator (τ_r), (c) controller input gain for the first order (k_s), (d) gain for the first order compensator (τ_s)

Fig. 13. The effect of applied voltage in NMPPF controller

Fig. 14. Comparison of the PPF, NIRC, and NMPPF controller performances

Table 8. Comparison of values and percentages the PPF, NIRC, and NMPPF controller performances

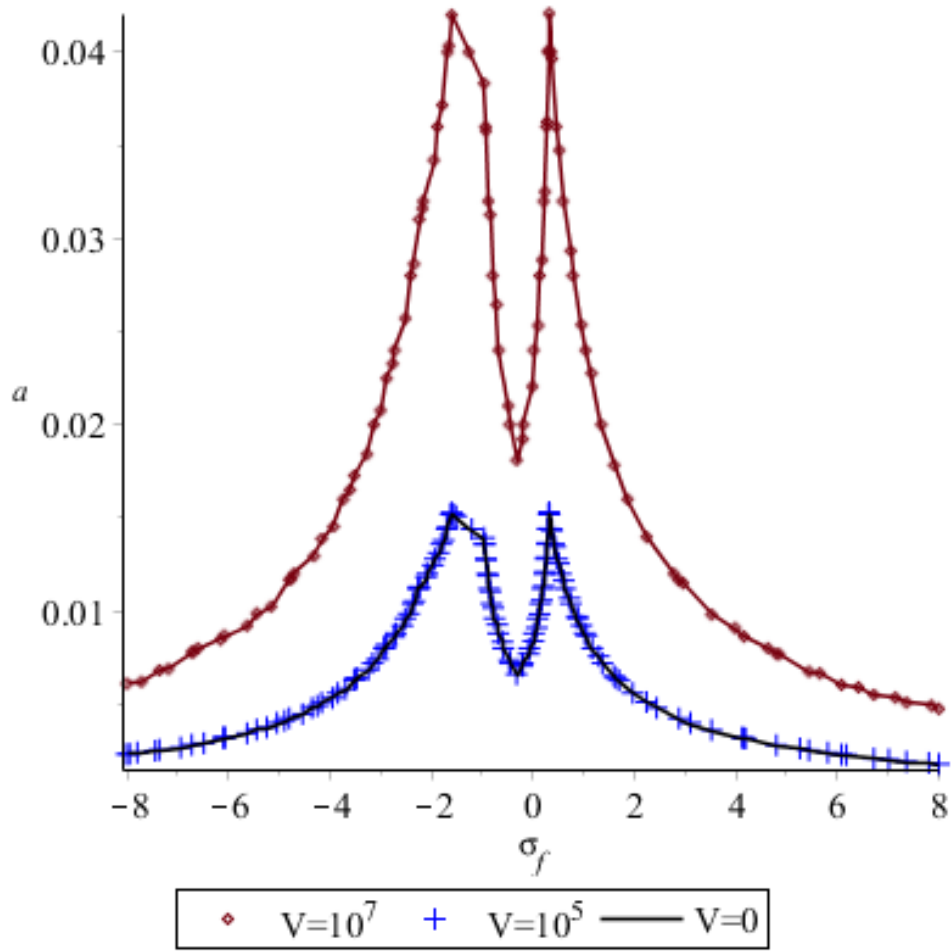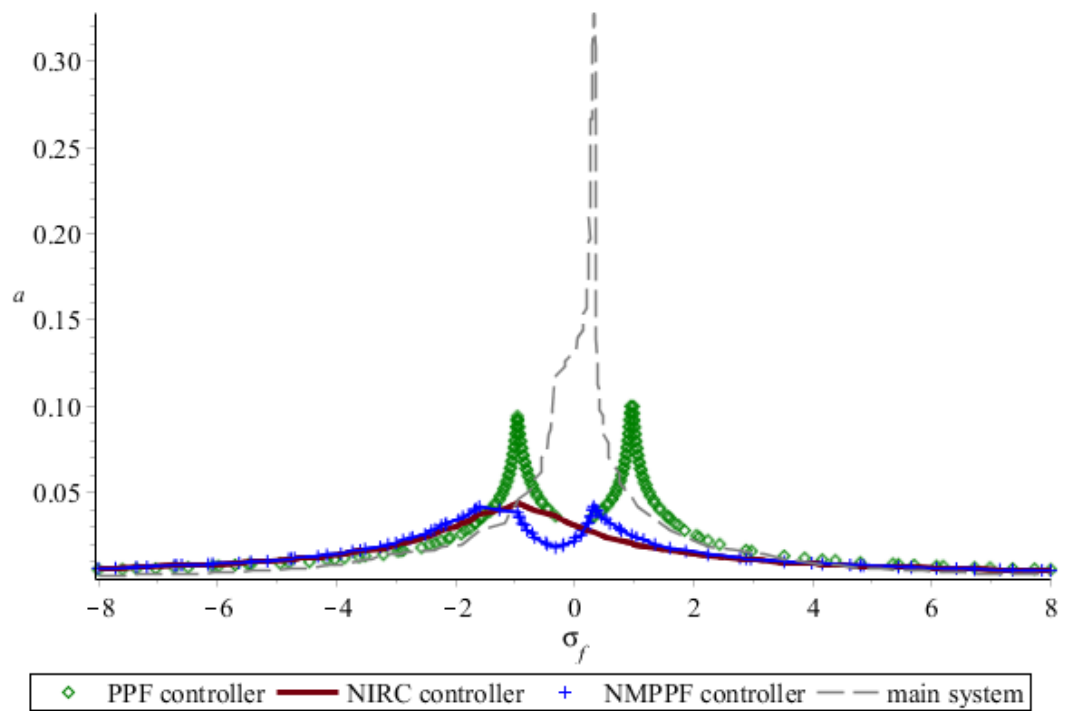| Controller	Amplitude	Improved performance compared to the main system
Main system	0.325	--
NMPPF	0.042	87.08%
PPF	0.10	69.23%
NIRC	0.044	86.46%

indicates the frequency response of the closed loop system with the PPF controller. The controller parameters are cited in Table 5. Implementation of PPF controller reduces vibration range in the resonant frequency region $\left(\sigma_f = 0\right)$. This controller amplifies the production of two-peak amplitudes with relatively large amplitude around the frequency. The amplitude in the resonant frequency reduced from $a = 0.32$ to $a = 0.1$ in the uncontrolled mode. Thus, one can state that it is suitable for controlling vibrations at resonant frequency, although it does not perform well around resonant frequency. The frequency response equations are as follows

$$\left(\frac{\hat{f}}{2}\right)^2 = \left[\left(\frac{\hat{\eta}_u}{2}\right)a + \frac{\hat{k}_p \hat{\eta}_p b^2}{2\lambda_p a}\right]^2 + $$

$$\left[\frac{3\hat{\alpha}}{8}a^3 - \frac{\hat{k}_p}{\hat{\lambda}_p}\left(\sigma_f\right)\frac{b^2}{a} - \sigma_f a\right]^2$$

(76)

$$\left[1 - \frac{\hat{\eta}_p^2}{\hat{\lambda}_p^2}\frac{b^2}{a^2}\right]^{\frac{1}{2}} = \frac{2}{\hat{\lambda}_p}\left(\sigma_f\right)\frac{b}{a}$$

(77)

An analysis of each control parameter is done for obtaining a better understanding of the effect of each parameter in response to improved system performance. The PPF controller is suitable for controlling the excitation amplitude at $\left(\sigma_f = 0\right)$. However, as shown in Figs. 5 and 6, the amplitude of the resonator is practically converted to two frequencies near the natural frequency (before and after) by applying this controller. Fig. 6 indicates the sensitivity of the amplitude response to changes in control parameters. Fig. 6(a) as the coefficient of damping increases, the amplitude of the vibrations decreases almost linearly. The controller input gain results indicated in Figs. 6(b) and 6(c) have similar effects. Increasing these parameters ends in more inhibition of the precise frequency value of the resonator. Although by increasing these two parameters the two peaks are separated, it is impossible to comment on the two peaks created. Fig. 6(c) shows that the controller behavior changes when $\lambda_p = 1$. As is seen in Fig. 6(d), the voltage change has a direct effect

on the amplitude of the resonator. By affecting the frequency, this parameter changes the other parameters. The following figure shows the increase in voltage that decreases the amplitude of the vibrations.

The analytical solution of this controller is given in **Appendix C.**

7.3. Nirc Controller Performance Analysis

In this section, the outcomes of applying NIRC control method on the smart plate is discussed. The NIRC consists of a first-order resonant integrator that provides additional damping in a closed-loop system response to reduce high amplitude nonlinear vibration around the fundamental resonance frequency. Numerical values of the NIRC controller are listed in Table 6. Fig. 7 shows the steady-state vibration amplitude versus changes in excitation frequency. Unlike conventional methods such as PPF and NMPPF, the graph shows small bending toward the negative side of the frequency axis. The NIRC controlled system exhibits no high-amplitude peak on either side of the fundamental mode in the frequency domain. Fig. 7 is obtained from the analytical solution Method of Multiple Scales such as the solution NMPPF. Next, the effects of three control variables on system response are examined. Fig. 8 shows the vibration amplitude of an NIRC controlled smart plate when control parameters are changed.

$$f^2 = \left[\hat{\eta}_u a + \frac{\hat{\lambda}\,\tau_v\,a}{2}\right]^2 + \left[\begin{array}{c}\frac{3\hat{\alpha}}{4}a^3 - \\ 2\left(\frac{\lambda\tau_v}{2} + \sigma_f\right)a\end{array}\right]^2$$

(78)

According to Fig. 8(a) increasing the positive values input gain controller λ, reduce domains. Negative values of this parameter causes the graph to bend to the right. In addition, reducing the negative values of the input gain λ will increase the vibration suppression. Fig. 8(b) shows the closed loop response of the system based on the variations in the input gain parameter, τ. Results demonstrate that as expected both gains have similar effect on the response. However, better suppression is achieved when both gains have the same signs. Fig. 9 shows the effect of the voltage on the amplitude of vibrations. As expected, increasing the voltage increases the amplitude of vibrations. The analytical solution of this controller is given in Appendix D.

7.4. Nmppf Controller Performance Analysis

Modulation Eqs. (74) and (75) were used to show the performance of the NMPPF controller on the smart plate. The numerical values of the parameters are selected in accordance with Table 7 for NMPPF controller. Fig. 10 shows the frequency response of NMPPF controlled systems. In this Fig., the right peak has higher amplitude than the left peak, but does not skip the amplitude.

By using this method not only the vibration reduces at the resonant frequency, but also the other two peaks have less amplitude than the PPF method. The maximum amplitude in NMPPF controlled system is much lower than the maximum peak in the controlled PPF response. NMPPF controller parameters, attenuation ratio and compensating frequencies, affect the closed loop system inhibition performance.

Moreover, the four control responses change the system response in the control process. Here the effect of these parameters on the system response is examined. The first parameter examined is μ_r. According to Fig. 11, the changes in parameter μ_r in the controller are such that with increase in its value, vibrations amplitude decreases. In the next step, the other benefits of the controller are examined.

Fig. 12 shows the second-order input variable k_r, the second-order output value τ_r, the first-order input compensator variable k_s, and the first-order output compensator interest τ_s. According to Fig. 12(a), the increase in k_r does not decrease the value of two peaks in the system response but makes them distance. Moreover, small k_r values do not reduce the magnitude of the two peak values. Nonetheless, with increase in k_r, the amplitude of the vibrations at the resonant frequency $(\sigma_f = 0)$ improves. As the second-order output τ_r increases in Fig. 12(b), the amplitude in the resonance frequency region decreases as a result of the inhibition of the vibration amplitude at frequency as Fig. 12(b) shows. Moreover, the two peak values occur at distances beyond the origin as the graphs become wider in the frequency range. Fig. 12(c) and Fig. 12(d) show the effect of first-order compensatory interest changes, k_s and τ_s. As already stated, second-order compensators have a better impact on amplification amplitude compared to second-order compensator diagrams. The increase in k_s increases the level of control of the controller that decreases the amplitude of the vibrations. The control gain function τ_s decreases with increase in parametric value of the system domain and the two peaks get distant like k_s.

Finally, evaluating the effect of voltage applied to the plate in the NMPPF controller, it is observed that increasing the voltage increases the amplitude of response.

Fig. 14 shows the frequency response of the uncontrolled system, system with PPF, NIRC, and NMPPF controllers for the excitation amplitude of $f = 0.09$. NPPF and NIRC controllers have a nearly similar effect on reducing amplitude at the resonant frequency. The PPF controller has a weaker performance than the other two controllers.

Appendix A

Airy function
where particular solution is considered as

$$\varphi_p = \widetilde{\varphi_1} \cos\left(\frac{2n\pi x}{a}\right) + \widetilde{\varphi_2} \cos\left(\frac{2m\pi y}{b}\right) + \widetilde{\varphi_3}\sin\left(\frac{n\pi x}{a}\right)\sin\left(\frac{m\pi y}{b}\right) \tag{A-1}$$

$$\widetilde{\varphi_1} = \frac{a^2 m^2 W_{mn}^2(t)}{32 b^2 n^2 A_{22}^*} = \varphi_1 W_{mn}^2(t).$$

$$\widetilde{\varphi_2} = \frac{b^2 n^2 W_{mn}^2(t)}{32 a^2 m^2 A_{11}^*} = \varphi_2 W_{mn}^2(t). \tag{A-2}$$

$$\widetilde{\varphi_3} = 0$$

A homogeneous solution form can be considered as

$$\varphi_h = C_1 x^2 + C_2 y^2 + C_3 xy \tag{A-3}$$

$$C_1 = -\frac{W_{mn}^2}{16}\left[\left(\frac{n\pi}{a}\right)^2 A_{12}^* - \left(\frac{m\pi}{b}\right)^2 A_{11}^*\right]$$

$$\left(A_{11}^* A_{22}^* - A_{12}^{*2}\right)^{-1} - \frac{N_{yy}^e}{2}$$

$$C_2 = \frac{W_{mn}^2}{16}\left[\left(\frac{n\pi}{a}\right)^2 A_{22}^* - \left(\frac{m\pi}{b}\right)^2 A_{12}^*\right] \tag{A-4}$$

$$\left(A_{11}^* A_{22}^* - A_{12}^{*2}\right)^{-1} - \frac{N_{xx}^e}{2}$$

$$C_3 = 0$$

Appendix B

The units in Table 9 are the coefficients of Eq. (31). These

Table 9. The units of the coefficients of transverse equation of the plate.

Constant	Z_1	Z_2	Z_3	Z_4
Unit	[M]	[MT^{-2}]	[ML^{-2}T^{-2}]	[MLT^{-2}]

units are in Newton SI version and lead to the unit kg m/s2.

Appendix C

Analytical solution of the controller PPF

we need new dimensionless variable for controllers so Eq. (38) becomes dimensionless like Eq. (36). The result is as follows

where

$$\eta_p = \frac{\tilde{\eta}_r}{\omega_r} \quad , \lambda_p = \frac{\hat{k}_p}{\omega_p^2} \tag{C-1}$$

To this end, two time-scales of $T_0 = t, T_1 = \varepsilon t$ are selected. Then, the time derivatives are defined as

$$\frac{d}{dt} = D_0 + \varepsilon D_1 + \dots \quad , \quad \frac{d^2}{dt^2} = \tag{C-2}$$
$$D_0^2 + 2\varepsilon D_0 D_1 + \dots$$

where $D_n = \frac{\partial}{\partial T_n}$ and $\varepsilon = \left(\frac{h}{\omega}\right)^2$ is a bookkeeping parameter. Eq. (C-2) is substituted in equation main system and controller that results in

$$D_0^2 U_0 + 2\varepsilon D_0 D_1 U_1 + \eta_U D_0 U_0 +$$
$$\varepsilon \eta_U D_1 U_1 + U_0 + \varepsilon U_1 + \alpha (U_0 + \varepsilon U_1)^3 + \dots \tag{C-3}$$
$$= f \cos(\Omega t) + \tau_r r + \tau_s s,$$

$$D_0^2 y + 2\varepsilon D_0 D_1 y + \eta_p D_0 y +$$
$$\varepsilon \eta_p D_1 y + y + \dots = \hat{\lambda}_p U \tag{C-4}$$

Parameters of the equations have to be scaled; therefore, parameters are set as:

$$\alpha = \varepsilon \hat{\alpha}, \lambda_p = \varepsilon \hat{\lambda}_p, k_p = \varepsilon \hat{k}_p, \eta_p = \varepsilon \widehat{\eta_p}, f = \varepsilon \hat{f} \tag{C-5}$$

Scaled parameters are substituted into the Eqs. (C-3), (C-4), then the variables $U(t), y(t)$ are expanded by

$$U(\varepsilon T_0, T_1) = U_0(T_0, T_1) + \varepsilon U_1(T_0, T_1) + \dots, \tag{C-6}$$

$$y(\varepsilon, T_0, T_1) = y_0(T_0, T_1) + \varepsilon y_1(T_0, T_1) + \dots \tag{C-7}$$

By placing above equations ordering the result in terms of the power of $\varepsilon^0, \varepsilon^1$ and ε^2, the following differential equations are obtained

$$O(\varepsilon^0): \quad D_0^2 U_0 + U_0 = 0 , \tag{C-8}$$

$$D_0^2 y_0 + y_0 = 0 , \tag{C-9}$$

$$O(\varepsilon^1): \quad D_0^2 U_1 + U_1 = \hat{f}\cos(\Omega t) + \hat{k}_p y_0$$
$$-2D_0 D_1 U_0 - \hat{\eta}_u D_0 U_0 - \hat{\alpha} U_0^3 , \tag{C-10}$$

$$D_0^2 y_1 + y_1 = \hat{\lambda}_p U_0 - 2D_0 D_1 y_0 - \hat{\eta}_r D_0 y_0 , \tag{C-11}$$

The equations of (C-8) and (C-9) are expressed as follows.

$$U_0 = A(T_1)e^{iT_0} + cc , \tag{C-12}$$

$$y_0 = B(T_1)e^{iT_0} + cc , \tag{C-13}$$

where $A(T_1)$ and $B(T_1)$ are complex parameters functions that will be defined by deface the secular terms, also where U_0 domain is r_0, which is a function of function

. Moreover, the term cc shows the complex conjugate function of its preceding sentences.

Next, Eqs. (C-12), (C-13) are substituted into the Eqs. (C-10) to (C-11). The simplified result is:

$$D_0^2 U_1 + U_1 = \hat{k}_p B(T_1)e^{iT_0} - \begin{pmatrix} \hat{\eta}_u A(T_1) + \\ 2D_1 A(T_1) \end{pmatrix}$$
$$ie^{iT_0} - \hat{\alpha} A^3(T_1)e^{i 3T_0} - 3\hat{\alpha} A^2 \overline{A} e^{iT_0} \tag{C-14}$$
$$+ \frac{\hat{f}}{2}e^{i\Omega T_0} + cc$$

$$D_0^2 y_1 + y_1 = \hat{\lambda}_p A(T_1)e^{iT_0}$$
$$- (\hat{\eta}_p B(T_1) + 2D_1 B(T_1))ie^{iT_0} \tag{C-15}$$

U_1 and y_1 are calculated using Eqs. (C-14) and (C-15) in time domain. For the system to have a bounded solution, it must be considered zero to the secular terms.

Next step is to sort Eqs. (C-14) and (C-15), and separate the secular terms,

$$\begin{bmatrix} \hat{k}_p B(T_1)e^{i\sigma_r T_1} \\ -\left(\hat{\eta}_u A(T_1)+2D_1 A(T_1)\right)i + \\ \dfrac{\hat{f}}{2}e^{i\sigma_f T_1}-A^2(T_1)\bar{A}(T_1)3\hat{\alpha} \end{bmatrix}e^{iT_0}=0 \tag{C-16}$$

$$\begin{bmatrix} \hat{\lambda}_p A(T_1)e^{-i\sigma_y T_r} \\ -\begin{pmatrix} \hat{\eta}_p B(T_1) \\ +2D_1 B(T_1) \end{pmatrix}i \end{bmatrix}e^{i\omega_y T_0}=0 \tag{C-17}$$

The solution to Eqs. (C-16) and (C-17) is assumed in the polar form of

$$A(T_1)=\frac{1}{2}a(T_1)e^{i\zeta_a(T_1)}, \tag{C-18}$$

$$B(T_1)=\frac{1}{2}b(T_1)e^{i\zeta_b(T_1)} \tag{C-19}$$

The real and imaginary parts will be separated and equal to zero by placing Eqs. (C-18) and (C-19) in Eqs. (C-16) and (C-17) The following equations are obtained.

$$D_1 a(T_1)=+\frac{\hat{f}}{2}\sin\left(\sigma_f T_1-\zeta_a(T_1)\right)+ \tag{C-20}$$
$$\frac{\hat{k}_p}{2}b(T_1)\sin\left(\zeta_b(T_1)-\zeta_a(T_1)\right)-\frac{\hat{\eta}_u}{2}a(T_1)$$

$$D_1\zeta_a(T_1)=\frac{3\hat{\alpha}}{8}a^2(T_1)$$
$$-\frac{\hat{f}}{2a(T_1)}\cos\left(\sigma_f(T_1)-\zeta_a(T_1)\right)- \tag{C-21}$$
$$\frac{\hat{k}_p b(T_1)}{2a(T_1)}\cos\left(\left(\zeta_b(T_1)-\zeta_a(T_1)\right)\right)$$

$$D_1 b(T_1)=-\frac{\hat{\eta}_p}{2}b(T_1)+\frac{\hat{\lambda}_p}{2}a(T_1) \tag{C-22}$$
$$\sin\left(\left(\zeta_a(T_1)-\zeta_b(T_1)\right)\right)$$

$$D_1\zeta_b(T_1)=\frac{\hat{\lambda}_p a(T_1)}{2b(T_1)}\cos\left(\begin{pmatrix}\zeta_a(T_1)\\-\zeta_b(T_1)\end{pmatrix}\right) \tag{C-23}$$

Since all variables of Eqs. (C-20) to (C-23) are time derivatives of function. New variables are defined, as follows to obtain the set of independent equations:

. by applying these changes, the modulation equation is obtained as follows.

$$\dot{a}=-\left(\frac{\hat{\eta}_u}{2}\right)a+\frac{\hat{f}}{2}\sin(\theta_a)+\frac{\hat{k}_p}{2}b\sin(\theta_a) \tag{C-24}$$

$$\dot{\theta}_a=-\frac{3\hat{\alpha}}{8}a^2+\frac{\hat{f}}{2}\frac{1}{a}\cos(\theta_a)$$
$$+\frac{\hat{k}_p}{2}\frac{b}{a}\cos(\theta_b)+\sigma_f \tag{C-25}$$

$$\dot{b}=-\frac{\hat{\eta}_p}{2}b-\frac{\hat{\lambda}_p}{2}a\sin(\theta_b) \tag{C-26}$$

$$\dot{\theta}_b=\frac{\hat{f}}{2}\frac{1}{a}\cos(\theta_a)+\left(\frac{\hat{k}_p b}{2a}-\frac{\hat{\lambda}_p a}{2b}\right)$$
$$\cos(\theta_b)-\frac{3\hat{\alpha}}{8}a^2 \tag{C-27}$$

steady-state conditions are considered to obtain the frequency response of the closed loop system. The coupled equations obtained for the frequency are the response of the main system and the controller domain.

$$\left(\frac{\hat{f}}{2}\right)^2=\left[\left(\frac{\hat{\eta}_u}{2}\right)a+\frac{\hat{k}_p\hat{\eta}_p b^2}{2\lambda_p a}\right]^2+$$
$$\left[\frac{3\hat{\alpha}}{8}a^3-\frac{\hat{k}_p}{\hat{\lambda}_p}(\sigma_f)\frac{b^2}{a}-\sigma_f a\right]^2 \tag{C-28}$$

$$\left[1-\frac{\hat{\eta}_p^{\;2}}{\hat{\lambda}_p^{\;2}}\frac{b^2}{a^2}\right]^{\frac{1}{2}}=\frac{2}{\hat{\lambda}_p}\left(\sigma_f\right)\frac{b}{a} \qquad \text{(C-29)}$$

Appendix D

Analytical solution of the controller NIRC

we need new dimensionless variable for controllers so Eq. (39) becomes dimensionless like Eq. (36). The result is as follows

where

$$\delta=\frac{h\tilde{\delta}}{\omega_Q}\;,\lambda=\frac{\tilde{\lambda}}{\omega_Q} \qquad \text{(D-1)}$$

To this end, two time-scales of $T_0=t, T_1=\varepsilon t$ are selected. Then, the time derivatives are defined as

$$\frac{d}{dt}=D_0+\varepsilon D_1+\dots\;,\qquad \frac{d^2}{dt^2} \qquad \text{(D-2)}$$
$$=D_0^2+2\varepsilon D_0 D_1+\dots$$

$$D_n=\frac{\partial}{\partial T_n}\;,\; \text{and} \quad \varepsilon=\left(\frac{h}{\omega}\right)^2$$

where is a bookkeeping parameter. Eq. (D-2) is substituted in equation main system and controller that results in

$$D_0^2 U_0+2\varepsilon D_0 D_1 U_1+\eta_U D_0 U_0+\varepsilon\eta_U D_1 U_1+$$
$$U_0+\varepsilon U_1+\alpha(U_0+\varepsilon U_1)^3+\dots=f\cos(\Omega t)+\tau_v v \qquad \text{(D-3)}$$

$$D_0 v+\varepsilon D_1 v+v+\dots=\lambda U-v^2 U^2 \qquad \text{(D-4)}$$

Parameters of the equations have to be scaled; therefore, parameters are set as: $\alpha=\varepsilon\hat{\alpha},\;\lambda=\hat{\lambda},\;\tau=\varepsilon\hat{\tau},\;\eta_u=\varepsilon\widehat{\eta_u},\delta=\hat{\delta},f=\varepsilon\hat{f}$.

Scaled parameters are substituted into the Eqs. (D-3), (D-4), then the variables U(t), v(t) are expanded by

$$U\left(\varepsilon,T_0,T_1\right)=U_0\left(T_0,T_1\right)+\varepsilon U_1\left(T_0,T_1\right)+\dots, \qquad \text{(D-5)}$$

$$v\left(\varepsilon,T_0,T_1\right)=\varepsilon v_0\left(T_0,T_1\right)+\varepsilon^2 v_1\left(T_0,T_1\right)+\dots. \qquad \text{(D-6)}$$

By placing above equations ordering the result in terms of the power of $\varepsilon^0,\varepsilon^1$ and ε^2, the following differential equations are obtained. Eq. (D-6) is chosen to be one order higher than the main system to keep the first-order dynamics of the controller at the same pace with the second-order nonlinear system model and to have all the necessary variables appear in the correct equations.

$$O\left(\varepsilon^0\right):\quad D_0^2 U_0+U_0=0\;, \qquad \text{(D-7)}$$

$$O\left(\varepsilon^1\right):\quad D_0^2 U_1+U_1=\hat{f}\cos\left(\Omega t\right)+ \qquad \text{(D-8)}$$
$$\tau v_0-2D_0 D_1 U_0-\hat{\eta}_u D_0 U_0-\hat{\alpha}U_0^3\;,$$

$$D_0 v_0+v_0=\lambda U_0-\delta^2 U_0^2 \qquad \text{(D-9)}$$

$$O\left(\varepsilon^2\right):\quad D_0 v_1+v_1=\lambda U_1-\delta^2 U_1^2-v_0\;. \qquad \text{(D-10)}$$

The equation of (D-7) is expressed as follows.

$$U_0=A\left(T_1\right)e^{iT_0}+cc\;, \qquad \text{(D-11)}$$

where $A(T_1)$ is complex-valued functions that will be defined by deface the secular terms, also where U_0 domain is r_0, which is a function of function T_1. shows the complex conjugate function of its preceding sentences. Eq. (D-11) is substituted into Eq. (D-9), and the ODE is solved. The solution to v_0 is found as

$$v_0=C\left(T_1\right)e^{-T_0}+\frac{\lambda}{2}\left(1-i\right)A\left(T_1\right)e^{iT_0}$$
$$-\frac{\delta}{5}\left(1-2i\right)A\left(T_1\right)e^{2iT_0}+2\delta^2 A\left(T_1\right)\bar{A}\left(T_1\right)+cc \qquad \text{(D-12)}$$

where $C(T_1)$ is going to be obtained in further steps of the solution. Next, Eqs. (D-11), (D-12) are substituted into the Eq. (D-8). The simplified result is:

$$D_0^2 U_1+U_1=\frac{\hat{f}}{2}e^{i\Omega T_0}-\left(\hat{\eta}_u A\left(T_1\right)+2D_1 A\left(T_1\right)\right)ie^{iT_0}$$
$$+\tau\left(C\left(T_1\right)e^{-T_0}+\frac{\lambda}{2}\left(1-i\right)A\left(T_1\right)e^{iT_0}\right)$$
$$-\hat{\alpha}A^3\left(T_1\right)e^{i3T_0}-3\hat{\alpha}A^2\bar{A}e^{iT_0}+$$
$$-\frac{\tau\delta^2}{5}\left(1-2i\right)A\left(T_1\right)e^{2iT_0}+2\tau\delta^2 A\left(T_1\right)\bar{A}\left(T_1\right)+cc \qquad \text{(D-13)}$$

U_1 is calculated using Eq. (D-8) in time domain. In order to solve for v_1, equation U_1 are substituted into Eq. (D-10) to form the ODE.

$$C\left(T_1\right)=c_v e^{\left(\left(\lambda-2\delta^2 G_5\right)\frac{\tau}{2}\right)T_1} \qquad \text{(D-14)}$$

$$\left[\begin{array}{l} \dfrac{\tau\lambda}{2}\left(\omega_s - i\right)A\left(T_1\right) - \left(\begin{array}{l} \hat{\eta}_u A\left(T_1\right) \\ +2D_1 A\left(T_1\right) \end{array} \right)i \\ +\dfrac{\hat{f}}{2}e^{i\sigma_f T_1} - A^2\left(T_1\right)\bar{A}\left(T_1\right)3\hat{\alpha} \end{array} \right]e^{iT_0} = 0 \qquad \text{(D-15)}$$

where c_v is a constant. The next objective is to obtain the modulation equation. For the system to have a bounded Eq. (D-13), it must be considered zero to the secular terms.

The solution to Eq. (D-15) is assumed in the polar form of

$$A\left(T_1\right) = \frac{1}{2}a\left(T_1\right)e^{i\zeta_a\left(T_1\right)}, \qquad \text{(D-16)}$$

The real and imaginary parts will be separated and equal to zero by placing Eq. (D-16) in Eq.(D-15) The following equations are obtained.

$$D_1 a\left(T_1\right) = -\frac{\tau\lambda}{2}a\left(T_1\right)$$
$$+\frac{\hat{f}}{2}\sin\left(\sigma_f T_1 - \zeta_a\left(T_1\right)\right) - \frac{\hat{\eta}_u}{2}a\left(T_1\right) \qquad \text{(D-17)}$$

$$D_1 \zeta_a\left(T_1\right) = \frac{3\hat{\alpha}}{8}a^2\left(T_1\right)$$
$$-\frac{\hat{f}}{2a\left(T_1\right)}\cos\left(\sigma_f\left(T_1\right) - \zeta_a\left(T_1\right)\right) - \frac{\lambda\tau}{2} \qquad \text{(D-18)}$$

Since all variables of Eqs. (D-17), (D-18) are time derivatives of T_1 function. New variables are defined, as follows to obtain the set of independent equations:
$\theta_a\left(t\right) = \sigma_f t - \zeta_a\left(t\right)$. by applying these changes, the modulation equation is obtained as follows.

steady-state conditions are considered to obtain the frequency response of the closed loop system. The coupled equations obtained for the frequency are the response of the main system and the controller domain.

$$f^2 = \left[\hat{\eta}_u a + \tau\lambda a\right]^2 + \left[\frac{3\hat{\alpha}}{4}a^3 - 2\left(\frac{\lambda\tau}{2} + \sigma_f\right)a\right]^2 \text{(D-19)}$$

8. CONCLUSIONS

In this article, active nonlinear vibrations control of a simply supported smart plate using the NMPPF controller was introduced. A piezoelectric layer is utilized for the control force implementation. The system response was also studied under NIRC and PPF control approaches. The nonlinear classical plate theory was considered and von-Karman strain–displacement field was used to model the plate. In the study of forced vibrations, first, the plate equation was analyzed without the controllers. Observations indicate that in this case, the frequency response curve in the $\sigma_f = 0$ zone has large resonance amplitude, in addition the jump phenomenon was observed. The produce the article show that by enhancing the excitation force, the response amplitude increases. A hardening phenomena was observed in the uncontrolled response of the smart plate. The plate with the controllers was analyzed using Multiple Scales Method All three controllers were analyzed using the Method of Multiple Scales. The solution contains the closed-loop responses of the NMPPF, NIRC and PPF approaches. Then stability analysis of the closed-loop system was performed and the sensibility of the parameters on the responses was compared.

The PPF controller had a weaker control effect than the other two controllers. Results show that increasing the gain and compensator damping coefficient decreases the peak values almost linearly. The NIRC provides additional damping for a closed loop system in the neighborhood of the resonant frequency. The nonlinear control term in addition to linear term provide more efficient control effect on the system. According to the studies, the performance of the NIRC controller has improved by 64.75% compared to the PPF controller. The NMPPF controller has a cubic nonlinear term in the second-order resonant compensator which provides better control for nonlinearity. This controller has a direct effect on the exact value of the resonant frequency. Vibration amplitudes at resonance are suppressed better as control gains and increases. The second-order compensator suppresses the exact resonant amplitudes better, also the first-order compensator induces more damping and higher gain values reduce the amplitude of the system. Results show that NMPPF controller reduced the vibration amplitude on a large bandwidth in the frequency domain better than the other two methods. The vibration suppression in this controller is 65.47% better than the PPF controller, almost 2.041% better compared to the NIRC controller.

REFERENCES

[1] E. Omidi, S.N. Mahmoodi, Nonlinear vibration control of flexible structures using nonlinear modified positive position feedback approach, in: Dynamic Systems and Control Conference, American Society of Mechanical Engineers, 2014, pp. V003T052A002.

[2] T. Zhang, H.G. Li, G.P. Cai, Hysteresis identification and adaptive vibration control for a smart cantilever beam by a piezoelectric actuator, Sensors and Actuators A: Physical, 203 (2013) 168-175.

[3] E. Pereira, S.S. Aphale, Stability of positive-position feedback controllers with low-frequency restrictions, Journal of Sound and Vibration, 332(12) (2013) 2900-2909.

[4] E. Omidi, N. Mahmoodi, Hybrid positive feedback control for active vibration attenuation of flexible structures, IEEE/ASME Transactions on Mechatronics, 20(4) (2014) 1790-1797.

[5] E. Omidi, R. McCarty, S.N. Mahmoodi, Implementation of modified positive velocity feedback controller for active vibration control in smart structures, in: Active and Passive Smart Structures and Integrated Systems 2014, International Society for Optics and Photonics, 2014, pp. 90571N.

[6] S.-Q. Zhang, Y.-X. Li, R. Schmidt, Active shape and vibration control for piezoelectric bonded composite structures using various geometric nonlinearities, Composite Structures, 122 (2015) 239-249.

[7] H. Tourajizade, M. Kariman, M. Zamanian, B. Firouzi, Optimal Control of electrostatically actuated micro-plate attached to the end of microcantilever, Engineering Mechchanics Journal of Amirkabir, 49(4) (2018) 131-140.

[8] H. Vaghefpour, Nonlinear Vibration and Tip Tracking of Cantilever Flexoelectric Nanoactuators, Iranian Journal of Science and Technology, Transactions of Mechanical Engineering, (2020) 1-11.

[9] L. Marinangeli, F. Alijani, S.H. HosseinNia, Fractional-order positive position feedback compensator for active vibration control of a smart composite plate, Journal of Sound and Vibration, 412 (2018) 1-16.

[10] N. Sepehrya, M. Ehsanib, M. Shamshirsazc, Free and Forced Vibration Analysis of Piezoelectric Patches Based on Semi-Analytic Method of Scaled Boundary Finite Element Method, (2019).

[11] O. Garcia-Perez, G. Silva-Navarro, J. Peza-Solis, Flexible-link robots with combined trajectory tracking and vibration control, Applied Mathematical Modelling, 70 (2019) 285-298.

[12] S. Azimi, A. Mazidi, M. Azadi, Active Flutter Control of a Swept Wing with an Engine by Using Piezoelectric Actuators, Persian, Amirkabir Journal of Mechanical Engineering,(DOI), 10 (2019).

[13] A. Andakhshideh, H. Karamad, Prediction and Control of Chaos in Nonlinear Rectangular Nano-plate on Elastic Foundation, AUT Journal of Mechanical Engineering, 52(5) (2019) 131-140.

[14] C. Zhu, X. Fang, J. Liu, A new approach for smart control of size-dependent nonlinear free vibration of viscoelastic orthotropic piezoelectric doubly-curved nanoshells, Applied Mathematical Modelling, 77 (2020) 137-168.

[15] C.-Y. Chia, Nonlinear analysis of plates, McGraw-Hill International Book Company, 1980.

[16] V. Birman, Plate structures, Springer Science & Business Media, 2011.

[17] A. Shooshtari, S. Razavi, Nonlinear vibration analysis of rectangular magneto-electro-elastic thin plates, International journal of engineering, 28 (2015) 136-144.

[18] A. Abe, Y. Kobayashi, G. Yamada, One-to-one internal resonance of symmetric crossply laminated shallow shells, J. Appl. Mech., 68(4) (2001) 640-649.

[19] A. Milazzo, An equivalent single-layer model for magnetoelectroelastic multilayered plate dynamics, Composite structures, 94(6) (2012) 2078-2086.

[20] J.N. Reddy, Theory and analysis of elastic plates and shells, CRC press, 1999.

[21] M. Rafiee, X. He, K. Liew, Nonlinear analysis of piezoelectric nanocomposite energy harvesting plates, Smart Materials and Structures, 23(6) (2014) 065001.

[22] E. Omidi, S.N. Mahmoodi, Sensitivity analysis of the nonlinear integral positive position feedback and integral resonant controllers on vibration suppression of nonlinear oscillatory systems, Communications in Nonlinear Science and Numerical Simulation, 22(1-3) (2015) 149-166.

[23] E. Omidi, S.N. Mahmoodi, Nonlinear integral resonant controller for vibration reduction in nonlinear systems, Acta Mechanica Sinica, 32(5) (2016) 925-934.

[24] A.H. Nayfeh, D.T. Mook, Nonlinear oscillations, John Wiley & Sons, 2008.